AEDC-TR-81-26

Boundary-Layer Transition Correlation on a Slender Cone in Wind Tunnels and Flight for Indications of Flow Quality

N. Sam Dougherty, Jr.
ARO, Inc.

David F. Fisher
NASA Dryden Flight Research Center

February 1982

Final Report for Period January 1970 – November 1978

ARNOLD ENGINEERING DEVELOPMENT CENTER
ARNOLD AIR FORCE STATION, TENNESSEE
AIR FORCE SYSTEMS COMMAND
UNITED STATES AIR FORCE

NOTICES

When U. S. Government drawings, specifications, or other data are used for any purpose other than a definitely related Government procurement operation, the Government thereby incurs no responsibility nor any obligation whatsoever, and the fact that the government may have formulated, furnished, or in any way supplied the said drawings, specifications, or other data, is not to be regarded by implication or otherwise, or in any manner licensing the holder or any other person or corporation, or conveying any rights or permission to manufacture, use, or sell any patented invention that may in any way be related thereto.

Qualified users may obtain copies of this report from the Defense Technical Information Center.

References to named commercial products in this report are not to be considered in any sense as an endorsement of the product by the United States Air Force or the Government.

This report has been reviewed by the Office of Public Affairs (PA) and is releasable to the National Technical Information Service (NTIS). At NTIS, it will be available to the general public, including foreign nations.

APPROVAL STATEMENT

This report has been reviewed and approved.

Keith L Kushman

KEITH L. KUSHMAN
Directorate of Technology
Deputy for Operations

Approved for publication:

FOR THE COMMANDER

Marion L. Laster

MARION L. LASTER
Director of Technology
Deputy for Operations

REPORT DOCUMENTATION PAGE

READ INSTRUCTIONS BEFORE COMPLETING FORM

1. REPORT NUMBER: AEDC-TR-81-26	2. GOVT ACCESSION NO.
3. RECIPIENT'S CATALOG NUMBER	
4. TITLE (and Subtitle): BOUNDARY-LAYER TRANSITION CORRELATION ON A SLENDER CONE IN WIND TUNNELS AND FLIGHT FOR INDICATIONS OF FLOW QUALITY	5. TYPE OF REPORT & PERIOD COVERED: Final Report, January 1970 - November 1978
	6. PERFORMING ORG. REPORT NUMBER
7. AUTHOR(s): N. Sam Dougherty, Jr., ARO, Inc., a Sverdrup Corporation Company, and David F. Fisher, NASA Dryden Flight Research Center	8. CONTRACT OR GRANT NUMBER(s)
9. PERFORMING ORGANIZATION NAME AND ADDRESS: Arnold Engineering Development Center/DOT Air Force Systems Command Arnold Air Force Station, Tennessee 37389	10. PROGRAM ELEMENT, PROJECT, TASK AREA & WORK UNIT NUMBERS: Program Element 65807F
11. CONTROLLING OFFICE NAME AND ADDRESS: Arnold Engineering Development Center/DOS Air Force Systems Command Arnold Air Force Station, Tennessee 37389	12. REPORT DATE: February 1982
	13. NUMBER OF PAGES: 46
14. MONITORING AGENCY NAME & ADDRESS(if different from Controlling Office)	15. SECURITY CLASS. (of this report): UNCLASSIFIED
	15a. DECLASSIFICATION/DOWNGRADING SCHEDULE: N/A

16. DISTRIBUTION STATEMENT (of this Report)

Approved for public release; distribution unlimited.

17. DISTRIBUTION STATEMENT (of the abstract entered in Block 20, if different from Report)

18. SUPPLEMENTARY NOTES

Available in Defense Technical Information Center (DTIC).

19. KEY WORDS (Continue on reverse side if necessary and identify by block number)

boundary-layer transition	conical bodies	transonic flow
wind tunnels	slender bodies	supersonic flow
flow quality	Mach numbers	
noise	Reynolds numbers	
flight data	subsonic flow	

20. ABSTRACT (Continue on reverse side if necessary and identify by block number)

Boundary-layer transition location measurements were made on a 10-deg sharp cone in 23 wind tunnels in the United States and Europe and in flight. The data were acquired at subsonic, transonic, and supersonic Mach numbers over a range of unit Reynolds numbers in an effort to obtain an improved understanding of the effect of wind tunnel flow quality on transition location. The data indicate that the transition mechanism in both wind tunnels and flight is associated with the formation of Tollmien-Schlichting waves in the

20. ABSTRACT, Concluded.

laminar boundary layer. However, the location of the end of transition was found to be primarily a function of the noise under the laminar boundary of the cone surface and, within ±20 percent, independent of Mach number and unit Reynolds number.

PREFACE

The research reported herein was conducted by the Arnold Engineering Development Center (AEDC), Air Force Systems Command (AFSC), and, in part, by the National Aeronautics and Space Administration (NASA) Dryden Flight Research Center (DFRC). The results were obtained by ARO, Inc., AEDC Division (a Sverdrup Corporation Company), operating contractor for the AEDC, AFSC, Arnold Air Force Station, Tennessee, under ARO Project Number P32A-P4A in cooperation with NASA/DFRC, Edwards Air Force Base, California. The Air Force Project Manager was Mr. Alexander F. Money. The NASA F-15 Test Program Manager was Mr. Terry Putnam. The NASA test pilots were Bill Dana and Einar Enevoldson. Data analysis was completed on June 15, 1979, and the manuscript was submitted for publication on November 2, 1979.

The correlations of experimental data obtained testify to the capable efforts of a large number of individuals at many different facilities who participated in these tests. Data presented herein were acquired in a spirit of cooperation with the NASA Langley Aeronautical Research Center, NASA Ames Research Center, the Naval Ship Research and Development Center, the Calspan Corporation, and the governments of the United Kingdom, France, and the Netherlands all participating.

This research was benefitted by the support, scrutiny, and critique of the U. S. Transition Study Group chaired by Dr. Eli Reshotko sought and received over a five-year period in all phases from test planning to final analysis of the results.

CONTENTS

ILLUSTRATIONS

TABLES

1.0 INTRODUCTION

Reynolds number scaling is a standard technique for extrapolating data obtained at a constant Mach number on scaled wind tunnel models to predict the full-scale prototype performance in flight. For Reynolds number scaling to be valid, both the model and full-scale bodies must be in thermal equilibrium since heat transfer has an influence on boundary-layer development. Many continuous flow wind tunnels simulating flight have a variable density capability wherein Reynolds number may be changed at constant Mach number and temperature by adjusting the pressure. A Reynolds number variation, thus obtained, can reveal variations in parameters upon which an extrapolation to flight Reynolds number might be based. However, Potter and Whitfield, Ref. 1, have shown that one cannot expect a constancy in the value of the boundary-layer transition Reynolds number relative to a characteristic length Reynolds number when scaling transition sensitive data. Furthermore, as pointed out by Morkovin, Ref. 2, there are no clear-cut rules to guarantee that predictions of transition location on general body shapes will be accurate. A common practice is to fix transition in the wind tunnel using artificial trip devices, particularly when there is a large mismatch in model-to-full-scale Reynolds numbers. Such a practice may provide a constancy in transition Reynolds number relative to the characteristic Reynolds number; however, the turbulent boundary-layer growth downstream of the trip may not be representative of natural growth, and thus the simulation is still inaccurate.

Experimenters, therefore, resort to empirical data corrections of some sort to improve their Reynolds number scaling techniques. These corrections are not universally applicable to different bodies and are not generally the same from one wind tunnel to another (e.g., Treon et al., Ref. 3). Tunnel-to-tunnel differences in data from the same body can arise from variations in wind tunnel flow quality. Three of the pertinent factors in wind tunnel flow quality are:

1. Nonuniformity in free-stream velocity (caused in part by wall interference),
2. Flow angularity (also caused in part by wall interference), and
3. Free-stream flow disturbances (acoustical noise and turbulence).

Research accelerated in each of these three areas in the last decade when the USAF and NASA jointly announced a technological need for improved definition of flow quality in production wind tunnels. The research reported herein is the result of one effort directed toward improving the understanding of the effects of free-stream noise on boundary-layer transition. Emphasis was in the Mach number range from 0.5 to 2.0.

2.0 APPROACH

Correlatable experimental data were acquired on a simple body in a number of wind tunnels and in flight at comparable test conditions. The parameters of concern were Mach number, Reynolds number, model incidence, and model adiabatic wall recovery temperature with constant body geometry. The body selected was a sharp, slender cone, which is second only to a sharp, flat plate in simplicity. The cone was felt to be more amenable to the planned experiments because a flat plate has difficult-to-hold manufacturing tolerances, can have three-dimensional effects because of its finite span, and can become structurally unstable at high dynamic pressures.

Laminar-turbulent transition location was selected as the primary dependent parameter for investigation because transition location is sensitive to the free-stream disturbance environment and to the free-stream unit Reynolds number. Zero axial surface pressure gradient, which is an ideal condition for a transition study, is approached along a slender cone at zero incidence. A 10-deg included angle cone (5-deg half angle) was selected which provided only slightly favorable pressure gradients at subsonic Mach numbers and a zero pressure gradient after bow shock attachment at $M_\infty \geq 1.025$.

Transition location is a naturally restless phenomenon ideally definable in the mean by a one-dimensional parameter (i.e., by the distance along a ray from the cone apex). Transition is a function of the receptivity of the laminar boundary layer to disturbances arising in the free-stream flow and on the surface of the body. Hence, the cone was kept highly polished throughout the investigation to minimize body-generated disturbances so that transition variations might, as closely as possible, reflect an influence of the flow environment.

Tests were conducted with the 10-deg cone using constant instrumentation in 23 wind tunnels in the U. S. and Europe. During these tests transition location and the noise disturbances reaching the cone surface were measured. Then, in order to evaluate the effects of the wind tunnel disturbance environment, transition data were acquired on the same cone in flight. The flight environment is not a zero disturbance environment; however, the lowest possible disturbance environment was obtained by placing the cone as far forward as possible on the nose boom of a test bed aircraft. The flight tests were performed in the air space over Edwards Air Force Base, California.

In contrast to the flight disturbance environment, which contains wind shears and pockets of vorticity along with whatever disturbances are caused by the aircraft itself (principally those from the propulsion system), the flow in a wind tunnel can contain a complex pattern of turbulence and aerodynamic noise peculiar to the given tunnel. In order

to relate transition occurrence in the wind tunnel to a disturbance environment, it was necessary to make some quantitative measurements of the flow disturbances. To fully characterize a given disturbance environment is an awesome task requiring many ensembles of three-dimensional spectra that possess inherent statistically nonstationary qualities. Full characterization was not attempted. However, two microphone measurements on the cone surface provided a partial quantification of disturbances actually reaching the cone surface (partial in that the measurements 1) were frequency-response limited, 2) provided only one-dimensional frequency spectra, and 3) could not distinguish whether the frequency components of pressure had their origin as noise or turbulence). In this sense, the experiments were of a relatively simple macroscopic nature which could be repeated in a large number of facilities over a broad range of test conditions but were lacking in the microscopic detail necessary to reveal the mechanics of any given transition observation. Two microphones were used to obtain redundancy in the measurement. In addition to the microphone measurements on the cone surface, a third microphone was used during the flight program to obtain measurements of the free-stream disturbances.

3.0 THE CONE AND EXPERIMENTAL TECHNIQUE

The 10-deg cone is made of stainless steel and is 44.5 in. long (Fig. 1). Transition was detected with a nominal 0.006-in. opening height pitot tube traversed in contact with the cone surface over a distance from 4 to 36 in. from the cone apex. The cone apex was less than 0.005-in. equivalent diameter. The cone surface finish was nominally 10 μin. RMS. The apex was checked repeatedly under a microscope, and the surface finish was checked

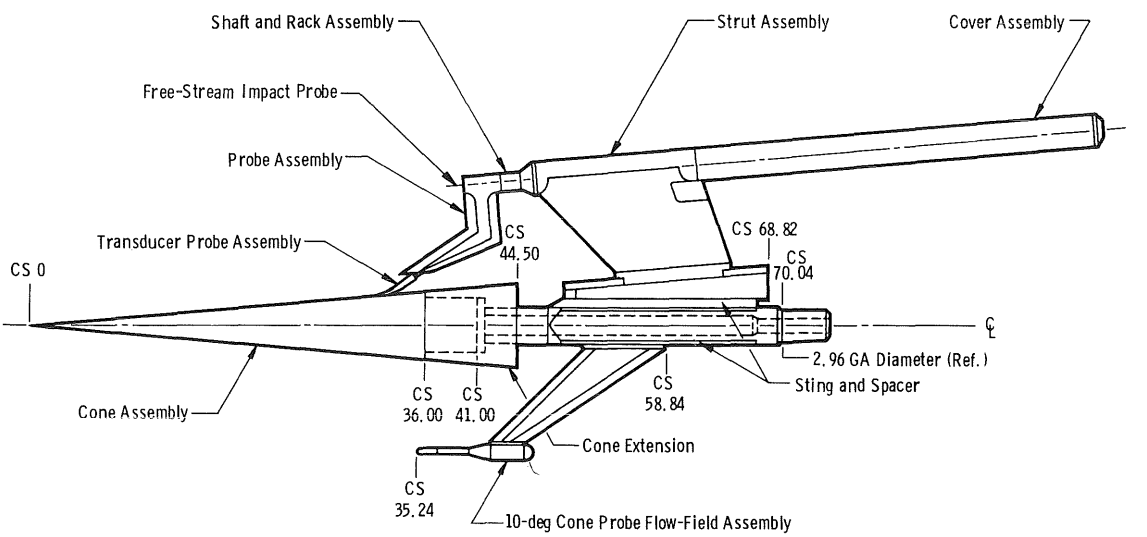

a. Elevation view

Figure 1. The instrumented cone.

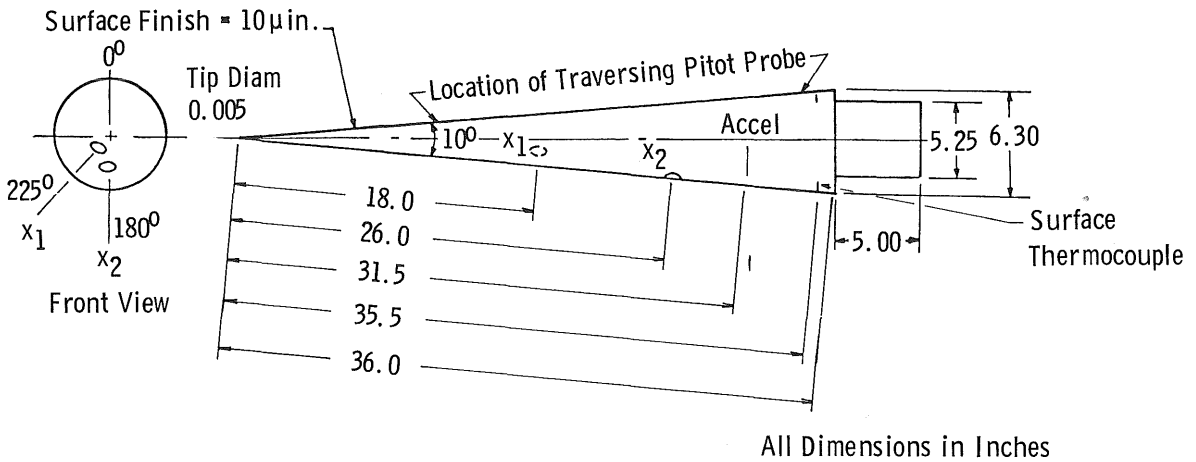

b. Instrument Locations
Figure I. Concluded.

repeatedly using a surface profilometer with a 500-μin. diamond-point stylus to assure the maintenance, as nearly as possible, of a constant geometric configuration. The cone and its instrumentation are described by Credle and Carleton in Ref. 4, and early results in six transonic tunnels are presented by Dougherty and Steinle in Ref. 5.

Tests were performed in 23 wind tunnels in the U. S. and Europe; the participating facilities are listed in Table 1. The results obtained in European wind tunnels in France, the Netherlands, and England are reported by Vaucheret in Ref. 6, by Ross and Rohne in Ref. 7, by Mabey in Ref. 8, and by Jordan in Ref. 9. A compilation of all the wind tunnel data with comparisons and a summary of results is given by Dougherty in Ref. 10. Details of the instrumentation and experimental techniques which, for the most part, became standardized are also related in Ref. 10.

The cone is shown in Fig. 2 on the F-15 test aircraft during flight tests at NASA/DFRC. The flight data are reported by Fisher and Dougherty in Ref. 11. The flight test matrix is shown in Fig. 3. The instrumentation and experimental techniques were essentially the same in the flight test program as in the wind tunnel investigation, except for the special considerations for flight test. The flight peculiar considerations were transducer selections for the wider temperature extremes of the flight test, pre-takeoff thermal conditioning of the cone to achieve adiabatic wall temperature during flight, the addition of an impact microphone on the traversing arm to measure the free-stream disturbances, and the corrections applied to the data to compensate for the inability to hold precisely zero incidence and adiabatic wall temperature. All of these considerations together with the calibrations performed for the flight test are reported in Ref. 11. The fixed flow-sensing probe seen beneath the cone in Figs. 1 and 2 measured Mach number, altitude, and incidence angle.

Table 1. Summary of Wind Tunnel Characteristics

Group	Tunnel	Distinguishing Geometry	Mach Number Range	Unit Reynolds Number Range x 10^{-6}	Predominant Disturbances	Resonant Mach Number	$\sqrt{\overline{p_s'^2}}/q_\infty$ max, percent	On-Line Recording Bandwidth of $\sqrt{\overline{p_s'^2}}/q_\infty$	Method of $\sqrt{\overline{p_s'^2}}/q_\infty$ Correction for Microphone Resonance[7]
1	NASA Langley 8 TPT	Slotted Wall	0.25 – 1.20	2.0 – 3.0	Low Frequency	0.80	2.20	0 – 60 kHz	No Corrections
	NASA Langley 16 TT	Slotted Wall	0.20 – 1.30	1.3 – 3.9	Low Frequency	0.82	3.60	0 – 60 kHz	No Corrections
	NASA Langley 16 TDT (Freon)[1]	Slotted Wall	0.30 – 1.15	1.5 – 3.7	Low Frequency	0.85	1.40	50 Hz – 60 kHz	No Corrections
	NSR&DC 7 x 10 T	Slotted Wall	0.20 – 1.13	1.5 – 4.0	Low Frequency	0.75	1.26	50 Hz – 60 kHz	No Corrections
	NLR 6.55 x 5.28 HST[2]	Slotted Wall	0.15 – 1.30	1.5 – 1.4	Compressor	0.80	1.01	50 Hz – 60 kHz	No Corrections
	RAE Farnborough 8 x 6[3,6]	Slotted Wall	0.20 – 1.19	0.4 – 2.5	Compressor	0.60	1.90	200 Hz – 60 kHz	No Corrections
	NASA Ames 12 PT	Solid Wall	0.20 – 0.90	2.0 – 3.0	Test Section	0.65	1.65	50 Hz – 60 kHz	No Corrections
	RAE Bedford 8 x 8 SWT (Subsonic Mode)	Solid Wall	0.20 – 0.80	0.25 – 3.0	—	None	0.80	50 Hz – 60 kHz	No Corrections
2	AEDC PWT Tunnel 4T	Perforated Wall	0.40 – 1.30	1.5 – 5.0	Edgetones	0.80/1.30	3.75	50 Hz – 60 kHz	No Corrections
	ONERA 6 x 6 S-2 Modane	Perforated Wall	0.25 – 1.30	2.0 – 7.2	Edgetones	0.80	2.77	50 Hz – 60 kHz	No Corrections
	ONERA 2.56 x 1.83 S-3 Modane[2,6]	Perforated Wall	0.25 – 1.00	2.0 – 12.5	Stilling Chamber	0.25	12.7	50 Hz – 60 kHz	No Corrections
	AEDC PWT Tunnel 16T	Perforated Wall	0.20 – 1.60	1.0 – 5.6	Edgetones	0.71	2.68	50 Hz – 60 kHz	See Footnote 8
	NASA Ames 11 TWT	Corrugated-Slot Wall	0.40 – 1.20	1.5 – 6.0	Slot Organ Pipe	0.75	2.00	50 Hz – 60 kHz	No Corrections
	NASA Ames 14 TWT	Corrugated-Slot Wall	0.40 – 1.05	2.6 – 4.0	Slot Organ Pipe	0.95	2.05	50 Hz – 60 kHz	No Corrections
	Calspan 8 TWT	Perforated Wall	0.60 – 0.95	2.0 – 3.0	Wall Tones	0.85	2.10	50 Hz – 60 kHz	No Corrections
	ARA, Ltd. Bedford 9 x 8[4]	Perforated Wall	0.21 – 1.40	1.5 – 4.4	Wall Tones	0.68	2.65	50 Hz – 60 kHz	No Corrections
3	RAE Bedford 8 x 8 SWT[5]	Converg/Diverg Nozzle	1.40 – 2.40	0.6 – 4.0	Wall Boundary Layer	None	0.45	50 Hz – 60 kHz	See Footnote 8
	NASA Langley 4 SPT	Converg/Diverg Nozzle	1.61 – 2.01	1.0 – 5.0	Wall Boundary Layer	None	0.12	50 Hz – 60 kHz	See Footnote 8
	AEDC PWT Tunnel 16S[6]	Converg/Diverg Nozzle	1.67 – 2.20	0.9 – 2.2	Wall Boundary Layer	None	0.50	0 – 60 kHz	No Corrections
	AEDC VKF Tunnel A	Converg/Diverg Nozzle	1.51 – 5.50	2.3 – 6.8	Wall Boundary Layer	None	—	—	—
	RAE Bedford 3 x 4 HSST	Converg/Diverg Nozzle	2.50 – 4.50	0.7 – 9.2	Wall Boundary Layer	None	0.20	50 Hz – 60 kHz	See Footnote 8
4	NASA Ames 9 x 7 SWT	Sliding-Block Nozzle	1.50 – 2.50	2.0 – 4.5	Wall Boundary Layer	None	0.18	50 Hz – 30 kHz	Cutoff Filter at 30 kHz
	NASA Langley 4 SUPWT (TS No. 1)	Sliding-Block Nozzle	1.60 – 2.86	1.5 – 5.0	Wall Boundary Layer	None	0.14	50 Hz – 60 kHz	See Footnote 8
	NASA Langley 4 SUPWT (TS No. 2)	Sliding-Block Nozzle	2.86 – 4.60	1.5 – 6.5	Wall Boundary Layer	None	0.24	50 Hz – 60 kHz	Cutoff Filter at 30 kHz

[1]Tests performed using both Freon and air as tunnel working fluid.

[2]Only noise data, no transition data.

[3]Results affected by model surface imperfections during this test.

[4]Transition data at Mach numbers from 0.2 to 0.6 only.

[5]Data acquired in Mach number range from 0.2 to 0.8 also.

[6]Data not included in Volume I but presented in Volume II, AEDC-TR-78-44, (Ref. 10).

[7]Effective bandwidth varies with sensor type, use of filters, and corrections for sensor diaphragm resonance when appropriate.

[8]Corrected per Table 1, AEDC-TR-78-44, Vol. I.

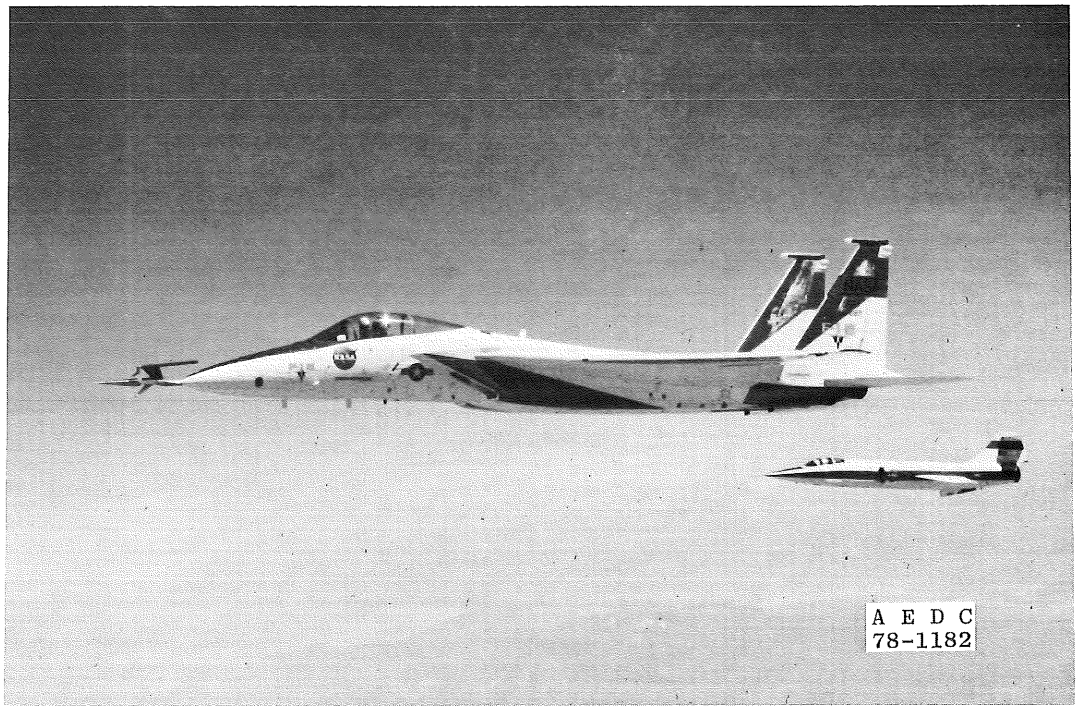

Figure 2. Cone mounted on the test aircraft.

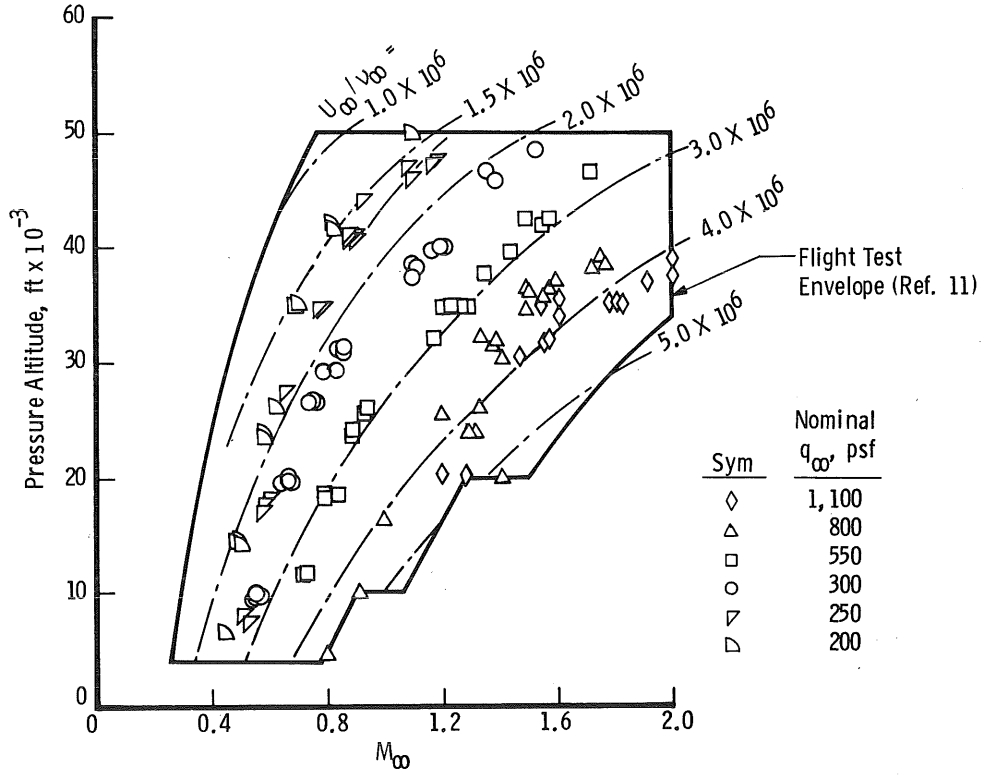

Figure 3. Matrix of flight test data.

The basic experimental technique in both wind tunnels and flight was first to acquire the disturbance environment data recorded by the two microphones on the cone surface, one at X_1 = 18 in., azimuthal angle 225 deg, the other at X_2 = 26 in., 180 deg from the ray traced by the pitot probe. The microphone data were recorded over a minimum 30-sec sampling period with the pitot probe in a retracted position an x usually from 33.5 to 35.5 in. Then the pitot probe was extended along the 0-deg ray until complete transition had been detected (within the limits of probe travel). The amount of extension was limited in the flight test to x = 16 in. because of pitot probe vibrations relative to the cone surface. The output of a triaxial accelerometer package mounted inside the cone was monitored for correcting the microphone data for acceleration sensitivity. Shaker table tests of the cone with the instrumentation installed revealed sensitivities primarily at 200 Hz and below. In the wind tunnels, recorded pressure fluctuations were generally at least an order of magnitude higher than the microphone response to the measured acceleration levels. Thus, no corrections for acceleration sensitivity were applied in the wind tunnels. Microphone signals were high-pass filtered at 200 Hz during playback of the flight test magnetic tape recording.

The pitot probe traversing rate in the wind tunnels was 12 in./min. In the flight test program a faster drive mechanism was utilized which increased the traverse rate to 38 in./min. During each data point in both the wind tunnels and in flight, time was allowed for the cone surface temperature to approach the adiabatic wall temperature before the data acquisition sequence was begun after Mach number, pressure altitude, and cone incidence were stabilized. Every effort was made to align the cone to the flow in the wind tunnels; occasional excursions in pitch and yaw were required to find the flow stream angle in some wind tunnels. Every effort was made by the pilot to trim the aircraft to align the cone to the airstream. The nose boom was pivotable to compensate for the aircraft angle-of-attack change with Mach number and altitude; vernier adjustments to Mach number or altitude were made by the pilot in an attempt to achieve simultaneously zero incidence and adiabatic wall temperature.

4.0 LAMINAR INSTABILITY

Data obtained in flight showed significant differences between the spectra obtained on the cone surface under laminar or turbulent boundary layers as well as differences from the free-stream impact probe. Representative data are shown in Fig. 4. For the condition shown, the traversing pitot probe data indicated that boundary-layer transition on the cone surface began at $Re_x = 4.23 \times 10^6$ and ended at $Re_x = 4.92 \times 10^6$. Thus, the forward microphone was located in the transition zone while the aft microphone was under a fully turbulent boundary layer. The turbulent boundary-layer spectrum had an integrated power approximately two orders of magnitude higher than the free-stream spectrum. The

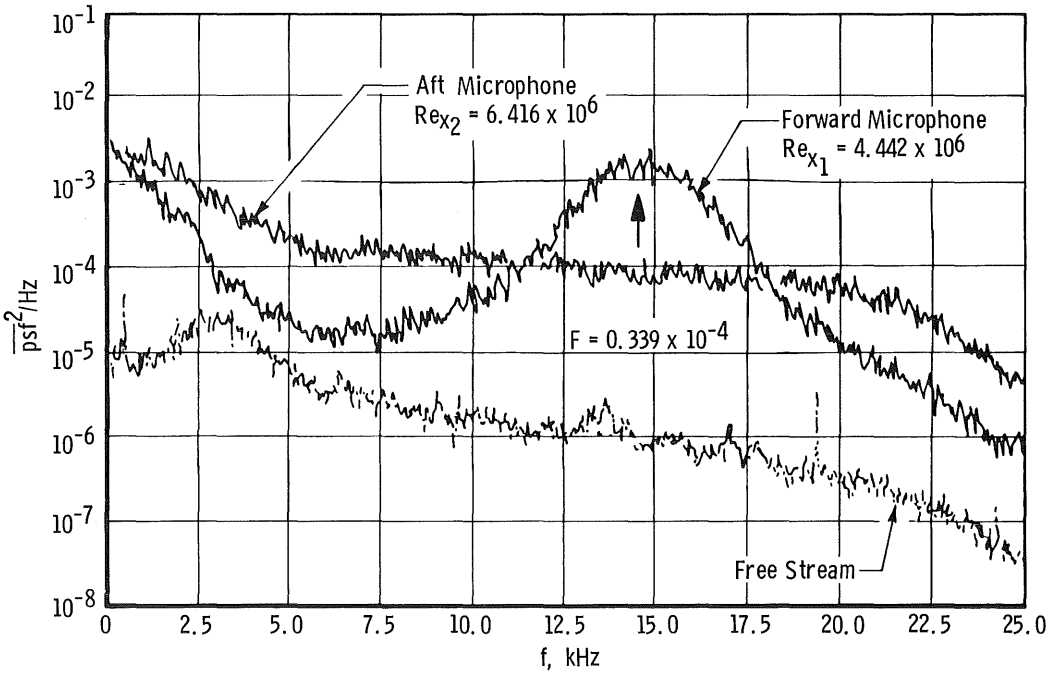

Figure 4. Comparison of cone-surface and free-stream impact microphone spectra.

transitional spectrum exhibited a pronounced peak at approximately 14.5 kHz, rising three orders of magnitude above the free stream. The parameter F denotes the value of a nondimensionalized frequency used by Mack in Ref. 12 which is defined as

$$F = \frac{2\pi f \nu_{e_o}}{U^2_{e_o}} \tag{1}$$

where f is the center frequency of the peak in Hz. The parameter F is a form of the Strouhal number in which unit Reynolds number provides the length scale for the nondimensionalization.

Smoothed spectra from the cone surface microphones in the form of nondimensionalized power, $\bar{p}'^2/q_\infty^2$, Hz^{-1}, are shown in Fig. 5 at $M_e \cong 0.80$ and $M_e \cong 1.35$. The parameter varied in Fig. 5 is Re_x obtained from flights at different altitudes at near-constant M_e. Spectral peaks are obvious under both laminar and transitional conditions, but disappear into a smooth spectrum when the boundary layer at the microphone location becomes turbulent. The events depicted in Fig. 5 are as follows:

1. As altitude was lowered at constant M_e, the transition location moved forward, passing one of the two microphone stations on the cone surface;

2. When the boundary layer was laminar, $Re_x < Re_t$, a characteristic spectral peak appeared at a relatively high frequency;

3. As the microphone Reynolds number increased, the spectral peak increased in power while decreasing in center frequency;

4. When the boundary layer became transitional, $Re_t < Re_x < Re_T$, the characteristic peak continued to decrease in frequency and increase in power, the rate of power increase being exponential with Re_x; there was also an accompanying increase in power at frequencies below about 6 kHz;

5. For $Re_x > Re_T$, the peak disappeared into a smoothly turbulent spectrum, and the power at low frequencies decreased below that of the transitional values. (A smooth spectrum free of peaks was construed as indicative of fully developed turbulent flow in this investigation.)

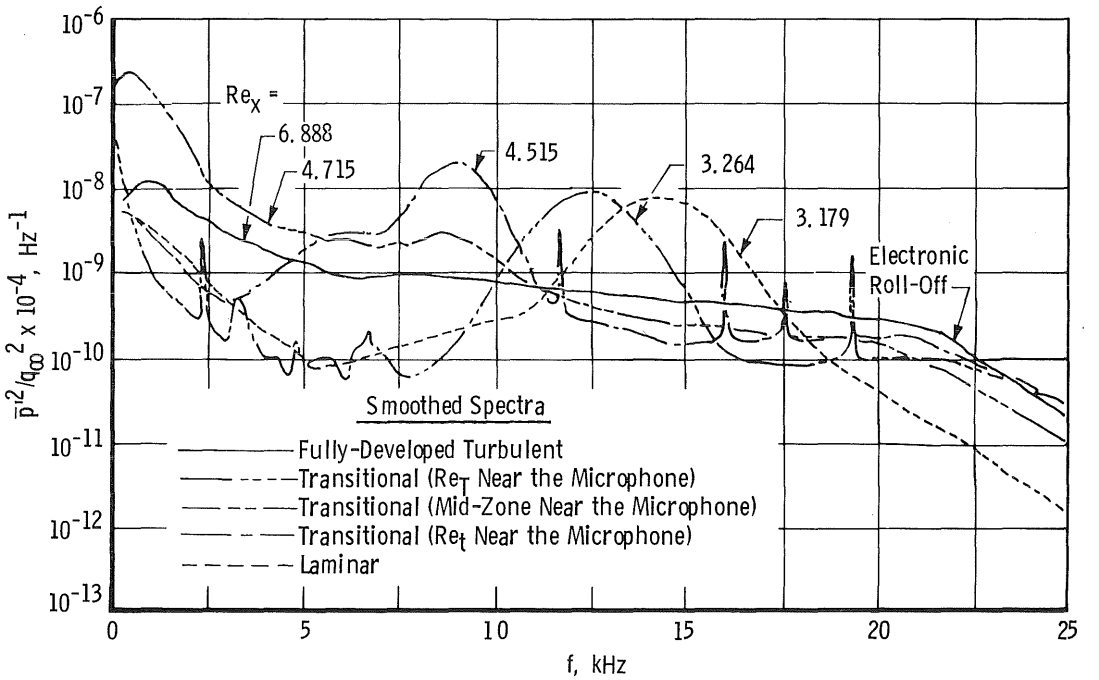

a. $M_e \cong 0.8$

Figure 5. Typical in-flight spectral data on the cone surface at varied Re_x.

As seen in Fig. 5, lesser peaks appeared randomly in the laminar and transitional spectra, but the predominant characteristic peaks contained substantially greater power and exhibited a monotonic variation with Re_x at constant M_e as shown in Fig. 6. All of the predominant spectral peak data obtained in flight are tabulated in Ref. 11.

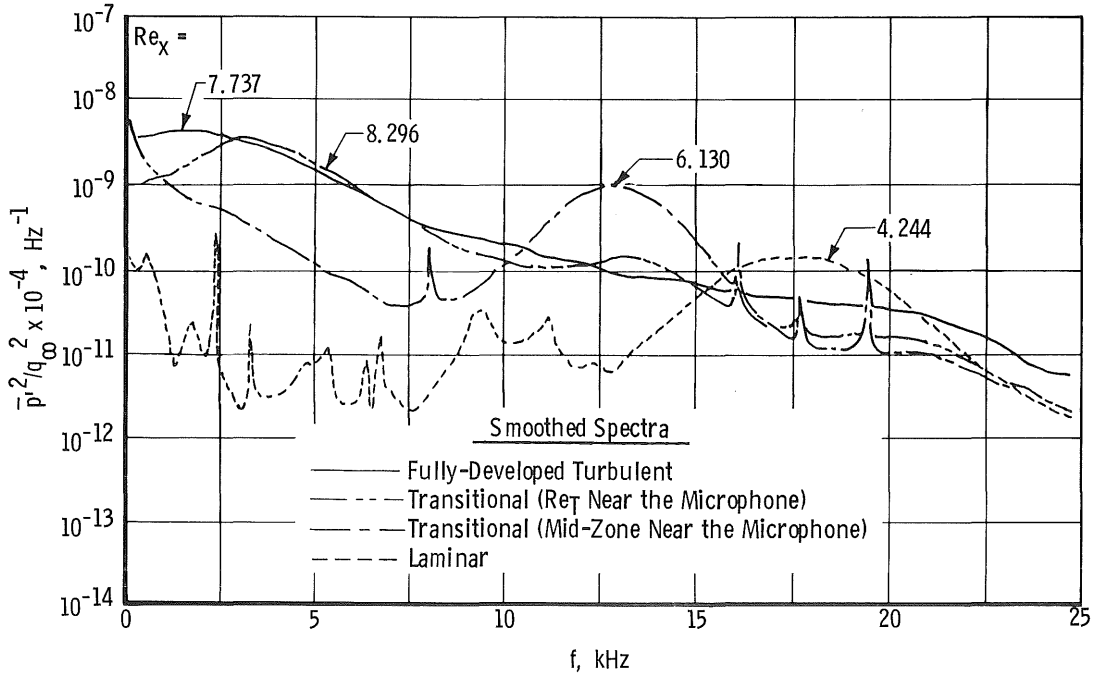

b. $M_e \cong 1.35$

Figure 5. Concluded.

Making use of the cone-planar similarity rule that $Re_{x_{cone}} = 3\ Re_{x_{PL}}$ for the boundary-layer properties, Mack's theoretical values of F in Ref. 12 at varied M_e for $\sqrt{Re_x} = 1{,}500$ were transformed to $\sqrt{Re_x} = 2{,}600$ for a cone and are shown in Fig. 6 in comparison with the cone flight data. Either the two-dimensional wave ($\psi = 0$) or the three-dimensional wave ($\psi \neq 0$) from Ref. 12 was used depending upon which gave the better agreement with the data at a particular Mach number. Mack's two-dimensional wave is the expected Tollmien-Schlichting mode of instability. The agreement between the measured frequencies on the cone and Mack's predicted frequencies, after cone-planar similarity transformation, seems good enough to conclude that the predominant mode of instability in flight before transition was the formation of Tollmien-Schlichting waves.

The flight test program was performed after completion of the wind tunnel investigation. The information revealed in the flight data were used in inspecting the microphone spectra obtained in the wind tunnels for any indications of Tollmien-Schlichting waves. Positive

examples were found in three wind tunnels, the NASA Langley 4-ft Supersonic Pressure Tunnel (SPT) and the two test sections of the NASA Langley 4-ft Supersonic Wind Tunnel (SUPWT). The better examples were at $M_\infty = 1.6$ and 2.0 in the 4 SPT, where the overall RMS amplitudes, $\sqrt{\overline{p'_s}^2}/q_\infty$, were the lowest recorded anywhere in the wind tunnel investigation. The spectral data recorded by the forward and aft microphones, respectively, while unit Reynolds number was varied at $M_\infty = 1.6$ are shown in Fig. 7. Broad peaks similar to those observed in the flight spectra are evident at $Re_{x_1} = 4.4 \times 10^6$ and $Re_{x_2} = 4.3 \times 10^6$. The overall aspects of spectral growth at high frequency experienced in flight, followed by amplitude growth at lower frequency when the boundary layer was transitional, followed by decay to a smoothly turbulent boundary-layer spectrum are evident in Fig. 7. Spectral data recorded in the 4 SPT at $M_\infty = 2.0$ are shown in Fig. 8. Spectral peaks are distinguishable at $Re_{x_1} = 4.4 \times 10^6$ and $Re_{x_2} = 4.2 \times 10^6$.

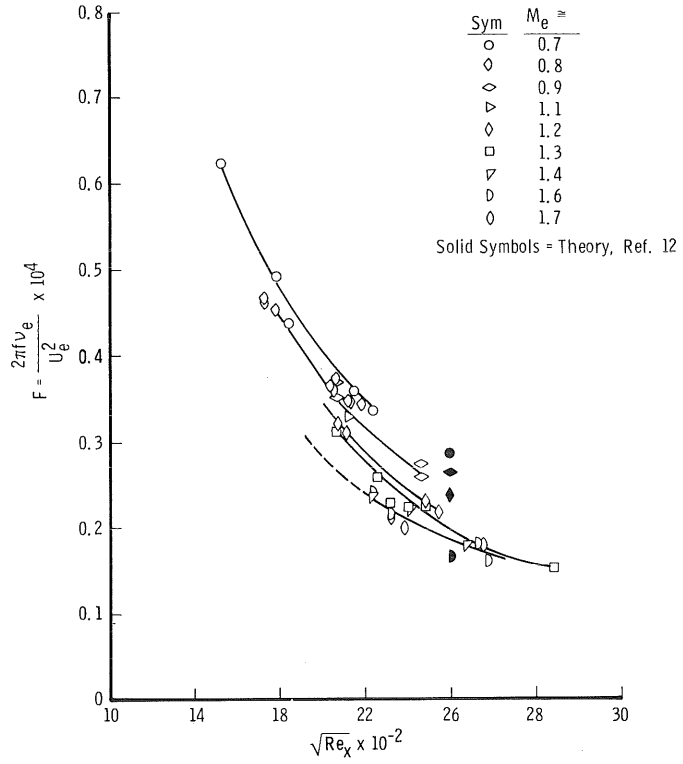

Figure 6. Variation of nondimensional frequency with $\sqrt{Re_x}$.

The expected peaks were less clearly distinguishable in the higher-disturbance environment of the NASA Langley 4 SUPWT at $M_\infty = 1.6$ and 2.0, Figs. 9 and 10, respectively. At $M_\infty = 1.6$ peaks can be discerned at $Re_{x_1} = 3.76 \times 10^6$ and at $Re_{x_2} = 4.34 \times 10^6$. At $M_\infty = 2.0$ a peak is apparent at $Re_{x_2} = 4.34 \times 10^6$.

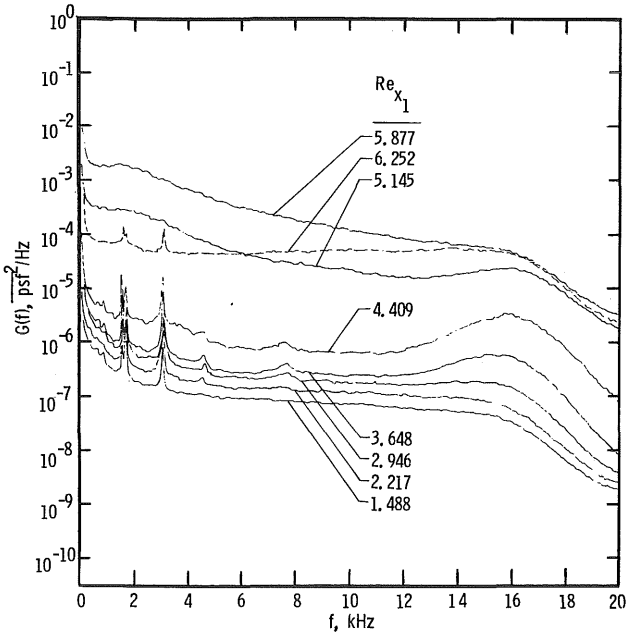

a. Forward microphone

Figure 7. Cone microphone spectra in the NASA Langley 4 SPT at M_∞ = 1.61 (M_e = 1.57).

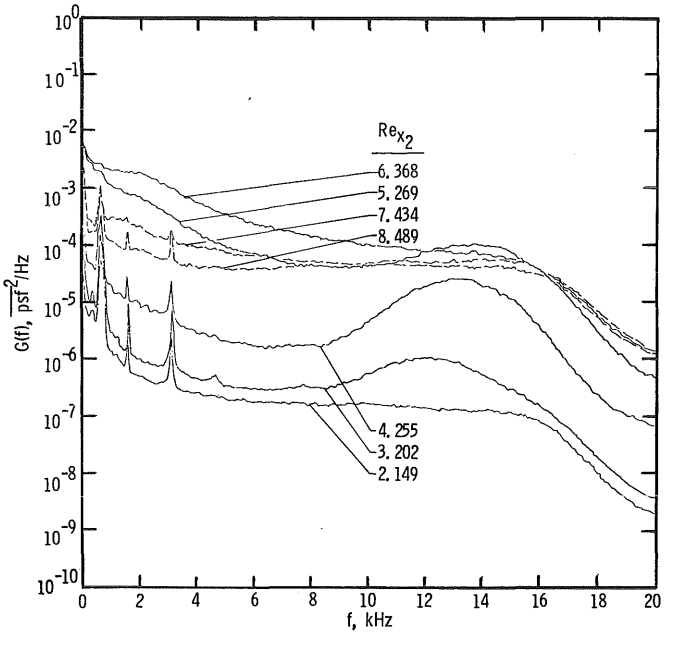

b. Aft microphone

Figure 7. Concluded.

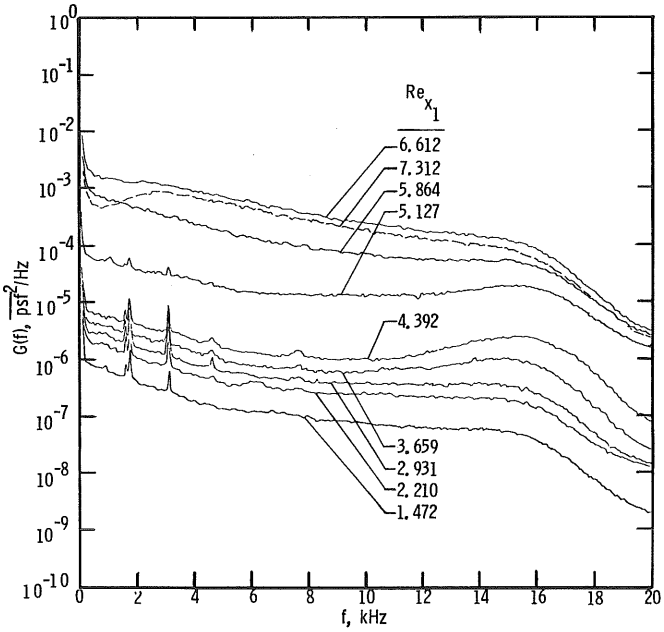

a. Forward microphone

Figure 8. Cone microphone spectra in the NASA Langley 4 SPT at M_∞ = 2.0 (M_e = 1.95).

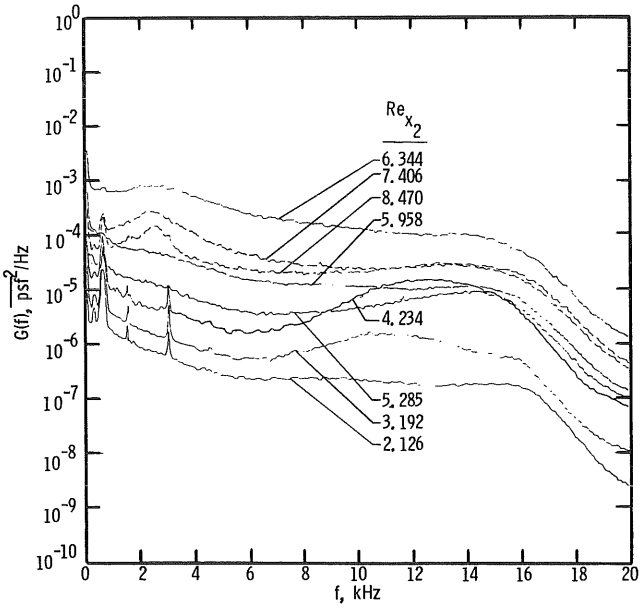

b. Aft microphone

Figure 8. Concluded.

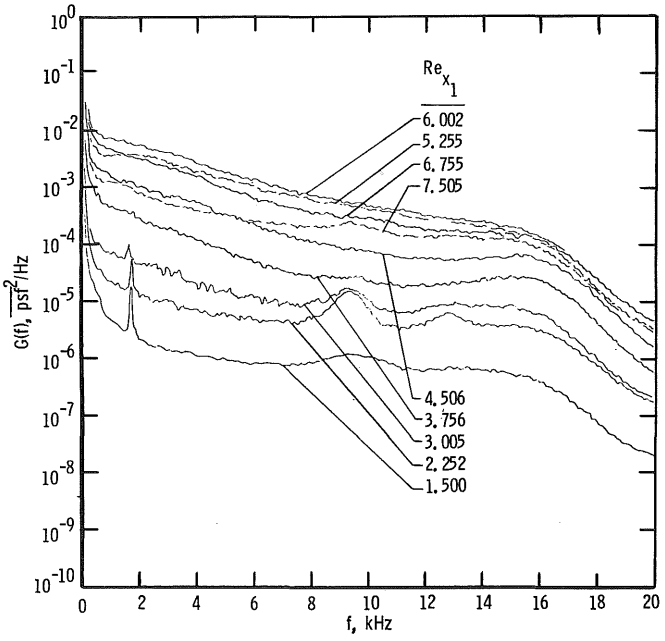

a. Forward microphone

Figure 9. Cone microphone spectra in the NASA Langley 4 SUPWT, test section No. 1, at M_∞ = 1.6 (M_e = 1.57).

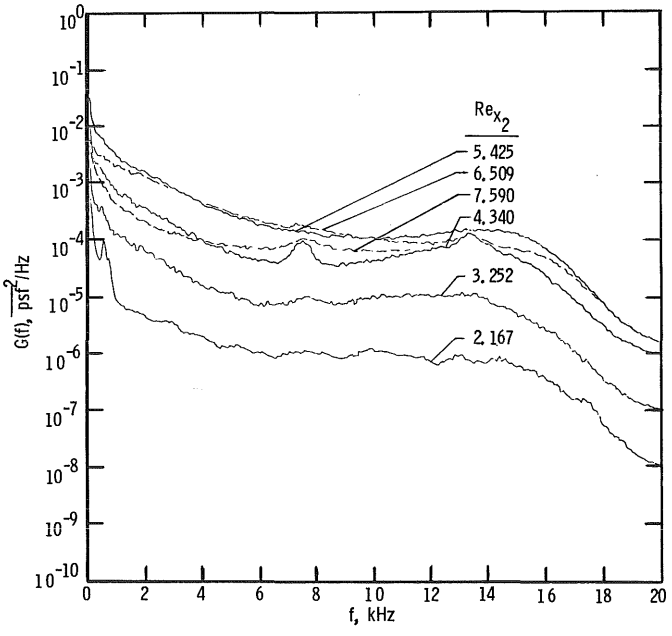

b. Aft microphone

Figure 9. Concluded.

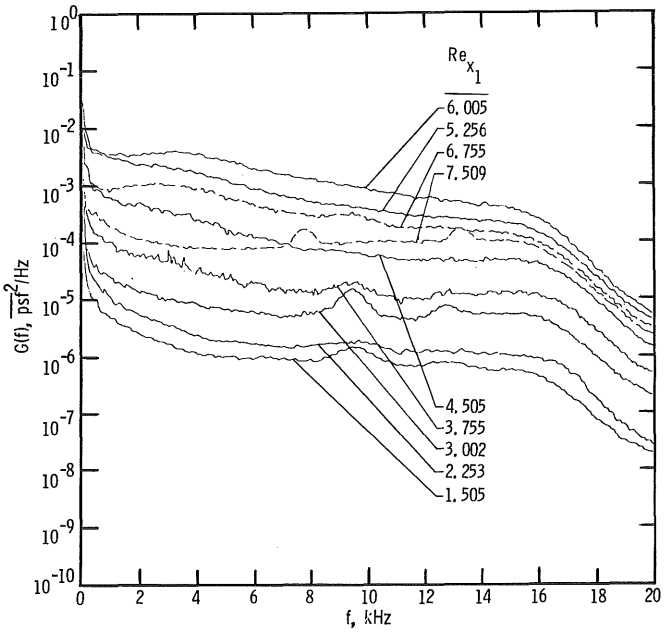

a. Forward microphone

Figure 10. Cone microphone spectra in the NASA Langley 4 SUPWT, test section No. 1, at M_∞ = 2.0 (M_e = 1.95).

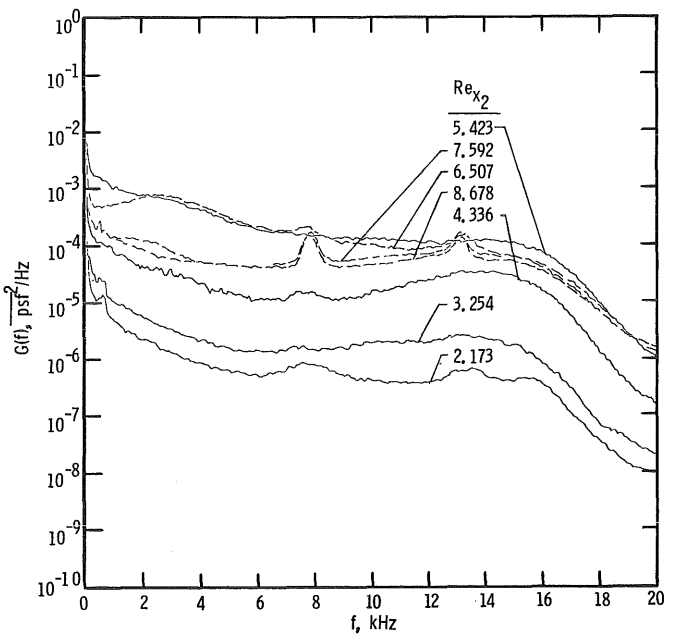

b. Aft microphone

Figure 10. Concluded.

At Mach numbers higher than about 2.0, microphone diaphragm resonance was experienced in the wind tunnels; this limited the flat frequency response range of the 1/4-in. condenser microphones. (The condenser microphones had been selected for their high sensitivity.) This problem was encountered at low free-stream static pressures and high supersonic speeds as described in Ref. 10. As the absolute values of the "unstable" frequencies approached a limiting diaphragm resonant frequency near 48 kHz, large sympathetic amplification resulted, with excessive indicated amplitude and an unnatural broadening of the spectral peak. The absolute amplitudes of overall RMS pressure, $\sqrt{p'^2}/q_\infty$, are questionable at the higher Mach numbers. Attempts to correct the resonance were not entirely successful, due to the inability to separate the degree of transducer amplification from the actual flow instability that was present. Nevertheless, spectral data obtained in the 4 SUPWT at $M_\infty = 3.5$, Fig. 11, and at $M_\infty = 4.6$, Fig. 12, indicate a peak at high frequencies although a clear center frequency for the peaks is difficult to distinguish.

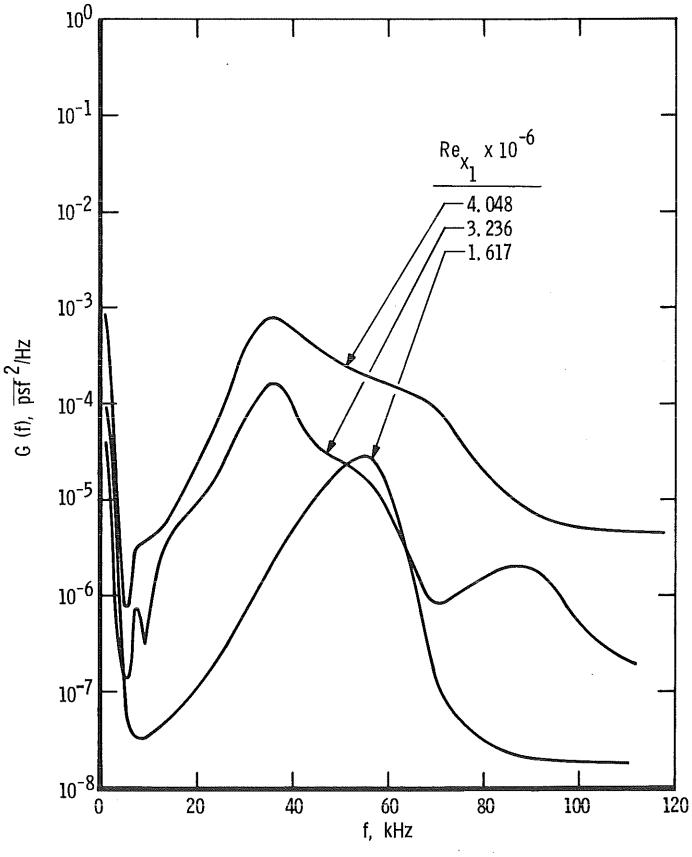

a. Forward microphone

Figure 11. Cone microphone spectra in the NASA Langley 4 SUPWT at $M_\infty = 3.5$ ($M_e = 3.37$).

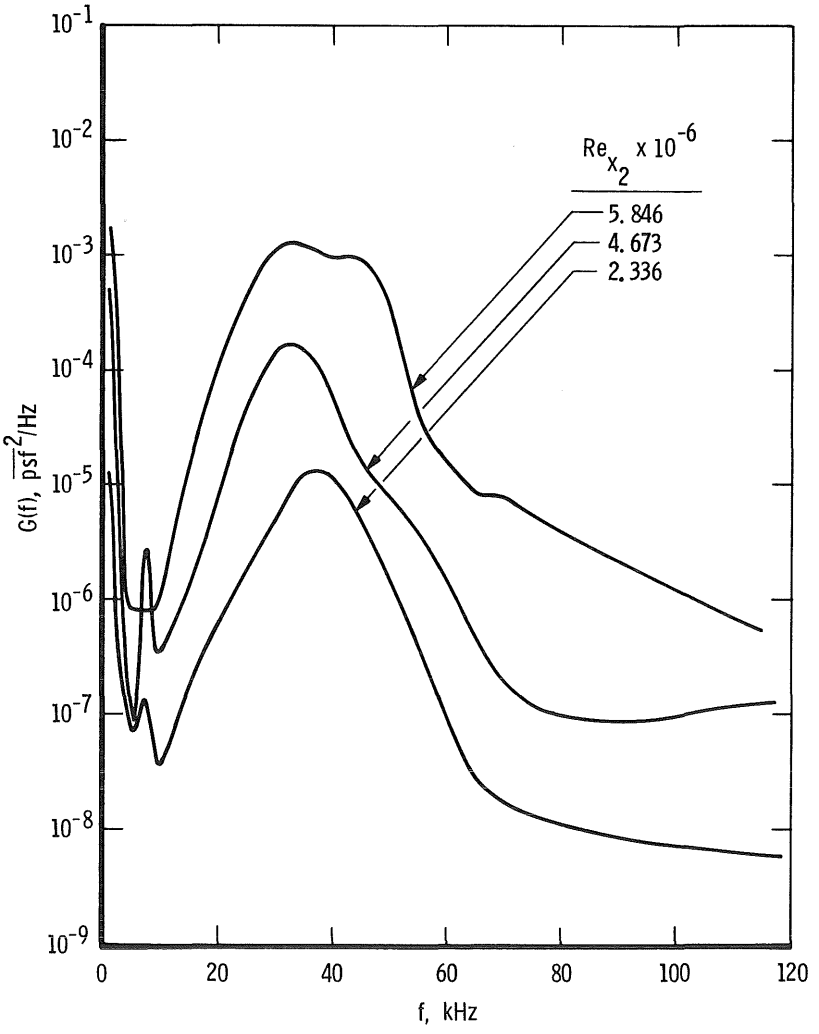

b. Aft microphone
Figure 11. Concluded.

The spectral peak data from the three wind tunnels are given in Table 2 with some reservations about the accuracy in defining peak center frequencies at the higher Mach numbers. The nondimensional peak frequency data for the three sets of data are compared with the flight data and Mack's theory in Figs. 13 and 14, revealing excellent agreement. Curiously, Mack's frequency for a two-dimensional wave appears to be in very close agreement at $M_\infty = 3.5$; however, the theory for a three-dimensional wave is in closer agreement with the data at $M_\infty = 4.6$.

The data from the NASA Langley wind tunnels yielded reasonable confirmation that the same type of instability was present in the wind tunnel and flight experiments. The

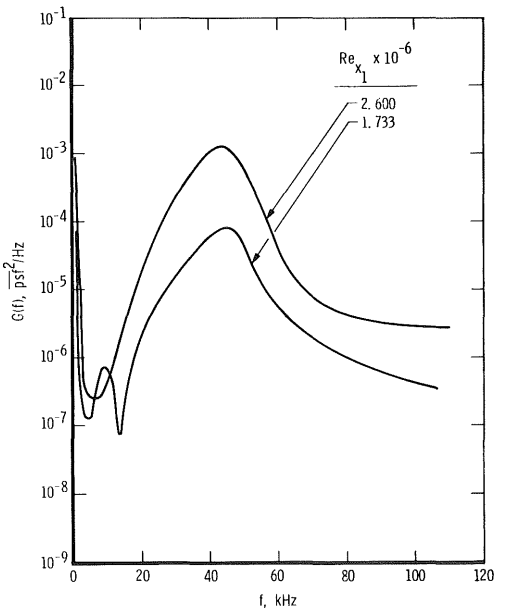

a. Forward microphone

Figure 12. Cone microphone spectra in the NASA Langley 4 SUPWT at $M_\infty = 4.6$ ($M_e = 4.36$).

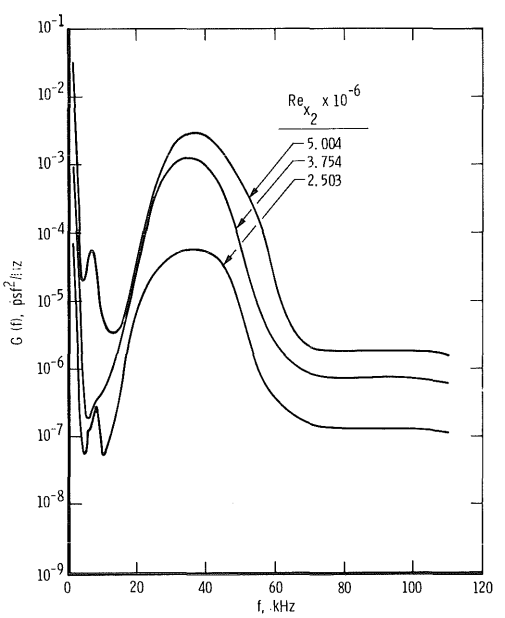

b. Aft microphone

Figure 12. Concluded.

Table 2. Spectral Peaks Detected in Supersonic Wind Tunnels

M_∞	M_e	$U_\infty/\nu_\infty \times 10^{-6}$	T_t, °R	U_e, fps	$\sqrt{Re_{x_1}}$	$F_1 \times 10^4$	$\sqrt{Re_{x_2}}$	$F_2 \times 10^4$
1.61	1.57	2.940	571.3	1,488	2,100	0.228		
1.61	1.57	1.964	571.3	1,488			2,063	0.286
1.61	1.57	2.432	571.3	1,488	1,910	0.273		
2.01	1.95	2.929	571.6	1,701	2,096	0.198		
2.01	1.95	1.955	571.6	1,701			2,058	0.244
			Data from the NASA Langley 4SPT					
1.60	1.56	2.504	610	1,549	1,938	0.261		
1.60	1.56	2.003	610	1,549			2,083	0.277
2.00	1.94	2.001	610	1,774			2,082	0.258
			Data from the NASA Langley 4SUPWT, TS No. 1					
*3.51	3.37	2.503	610	2,255	2,012	0.394		
↓	↓	2.503	↓	↓			2,418	0.336
		2.001			1,799	0.413		
		2.001					2,162	0.426
		1.000			1,272	0,534		
		1.000					1,528	0.956
*4.60	4.36	2.051	635	2,458			2,237	0.398
↓	↓	1.539	↓	↓	1,612	0.656		
		1.539					1,938	0.524
		1.026			1,316	1.007		
		1.026					1,582	0.797
			Data from the NASA Langley 4SUPWT, TS No. 2					

*These data are provisional since there are questions introduced by sympathetic microphone diaphragm resonance.

presence of the "Tollmien-Schlichting" instability could not be verified in the microphone data in any of the other wind tunnels because the amplitude of the disturbance values was much higher than in the Langley tunnels and thus obscured any Tollmien-Schlichting waves. However, the empirical relations derived from the flight data, Ref. 11, provided a basis for estimating the Tollmien-Schlichting frequency expected in the wind tunnels at typical operating temperatures. An estimated frequency of the instabilities expected at the two microphone locations for $0.5 \leq M_e \leq 2.0$ is given in Table 3.

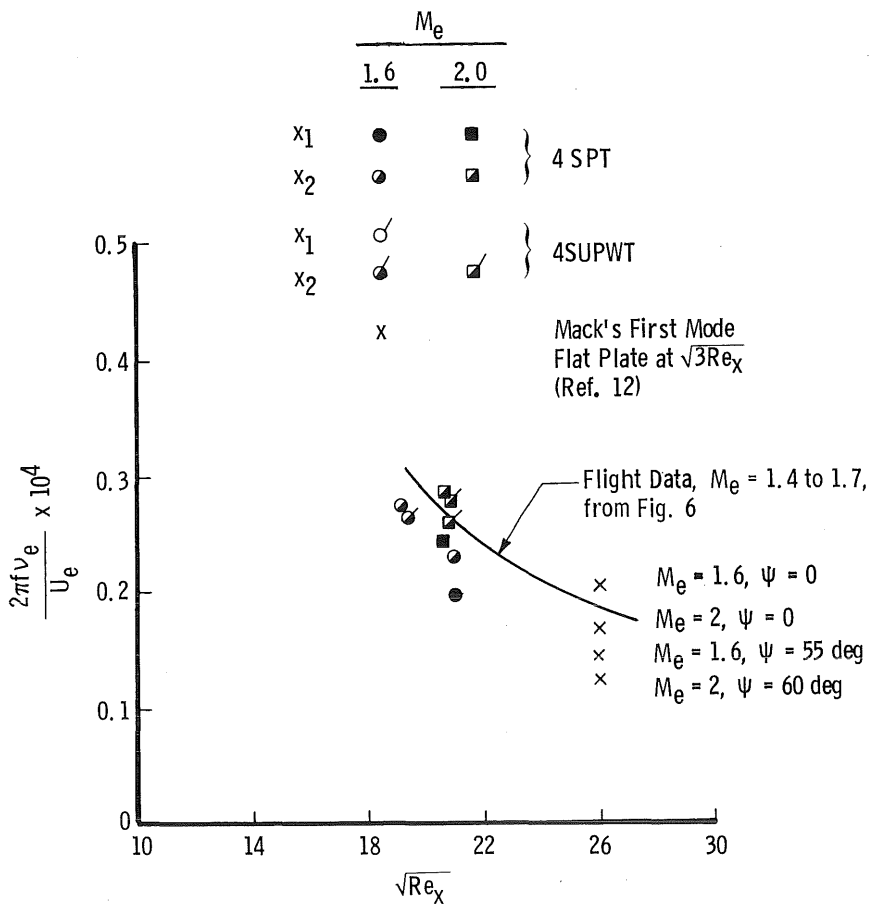

Figure 13. Nondimensional frequencies versus $\sqrt{Re_x}$ in the Langley Tunnels at M_e = 1.6 and 2.0.

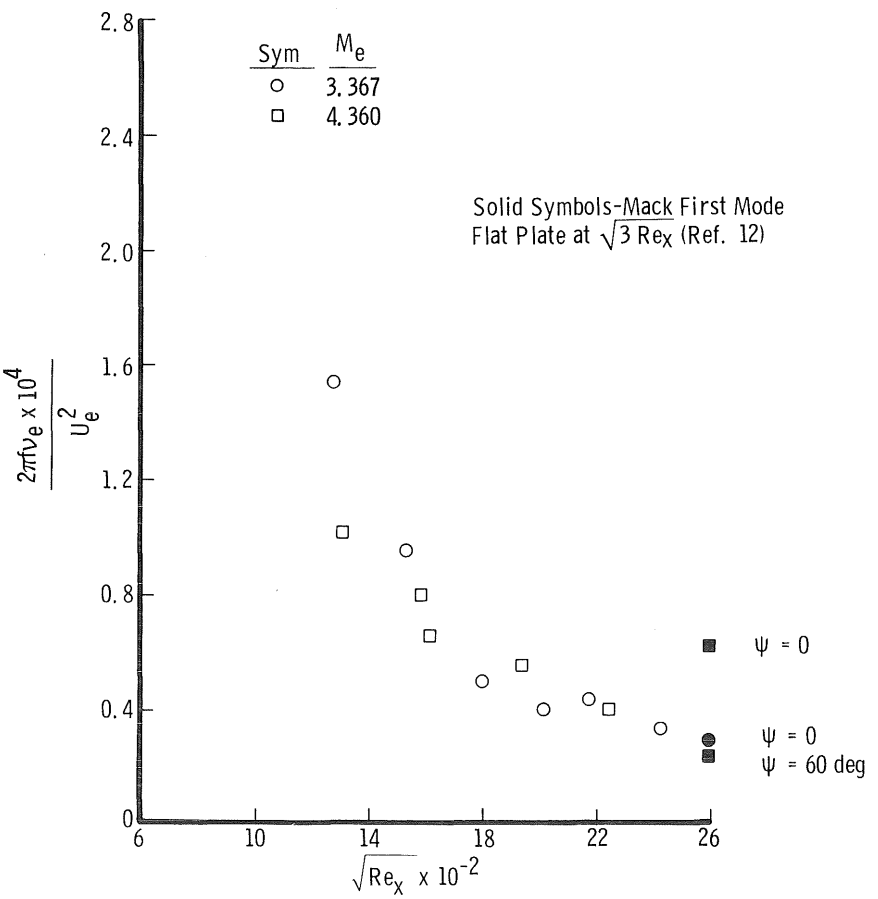

Figure 14. Nondimensional frequency versus $\sqrt{Re_x}$ from NASA Langley 4 SUPWT, test section No. 2.

Table 3. Estimated Tollmien-Schlichting Frequencies in Wind Tunnels

M_∞	M_e	$U_\infty/\nu_\infty \times 10^{-6}$	$U_e/\nu_e \times 10^{-6}$	U_e, fps	T_t, °R	$\sqrt{Re_{x_1}}$	$F_1 \times 10^4$	f_1, kHz	$\sqrt{Re_{x_2}}$	$F_2 \times 10^4$	f_2, kHz
2.00	1.942	3.000	3.066	1,719	572	2,145	0.194	16.27	2,577	0.134	11.24
2.00	1.942	2.000	2.044	1,719	572	1,751	0.291	16.27	2,104	0.202	11.30
1.50	1.458	3.000	3.024	1,432	572	2,130	0.268	18.47	2,560	0.186	12.82
1.50	1.458	2.000	2.016	1,432	572	1,739	0.402	18.47	2,090	0.278	12.77
1.25	1.212	3.000	3.000	1,236	560	2,121	0.306	18.06	2,550	0.212	12.51
1.25	1.212	2.000	2.000	1,236	560	1,732	0.460	18.10	2,082	0.318	12.51
1.00	0.961	3.000	2.991	1,024	560	2,118	0.345	16.82	2,546	0.239	11.65
1.00	0.961	2.000	1.994	1,024	560	1,729	0.518	16.83	2,079	0.358	11.63
0.75	0.740	3.000	2.970	815	560	2,110	0.368	14.17	2,537	0.276	10.63
0.75	0.740	2.000	1.980	815	560	1,723	0.504	12.94	2,071	0.378	9.71
0.50	0.494	3.000	2.970	549	540	2,110	0.423	10.98	2,537	0.317	8.09
0.50	0.494	2.000	1.980	549	540	1,723	0.580	9.87	2,071	0.435	7.40

5.0 TRANSITION

Various methods used to detect the location of transition will give different results as reported by Potter and Whitfield, Ref. 13. A chief difficulty among transition investigations has been the inability to establish a clearly defined "single" location that could be called the transition point. One method commonly used to ensure a consistent definition of transition location uses the surface traversing pitot probe, which was employed exclusively in the studies reported herein. A typical pitot pressure traverse profile obtained in flight on the cone surface is shown in Fig. 15. In the present investigation the point denoted by X_T was designated the end of transition, and the point X_t was designated the onset of transition. Both points were documented in terms of the end and onset of transition Reynolds numbers defined, and used, in Refs. 10 and 11 as $Re_T = U_e X_T/\nu_e$ and $Re_t = U_e X_t/\nu_e$. In this report, Re_T is chosen exclusively for the correlations. This is the same Re_T correlated by Pate and Schueler in Ref. 14 and by Pate in Ref. 15; hence, the present definitions are consistent with those measurements.

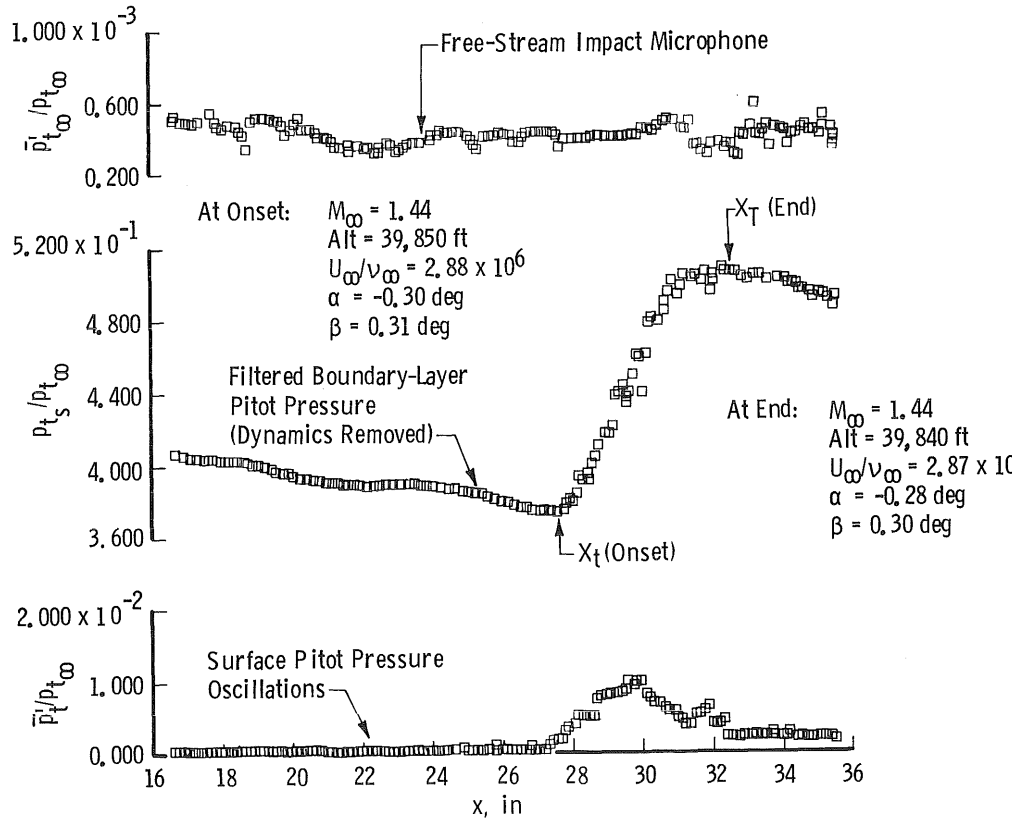

Figure 15. Typical in-flight pitot pressure profile.

5.1 FLIGHT REFERENCE DATA

The transition Reynolds numbers measured on the cone in flight are presented as a function of M_e in Fig. 16. These data have been corrected for deviations from zero incidence angle and adiabatic wall temperature at the time of data acquisition as outlined in Ref. 11. The different symbols used in Fig. 15 relate to how the flight tests were performed and are consistent with the symbols in Fig. 3. For approximately constant U_e/ν_e, transition location moved monotonically aft as M_e increased.

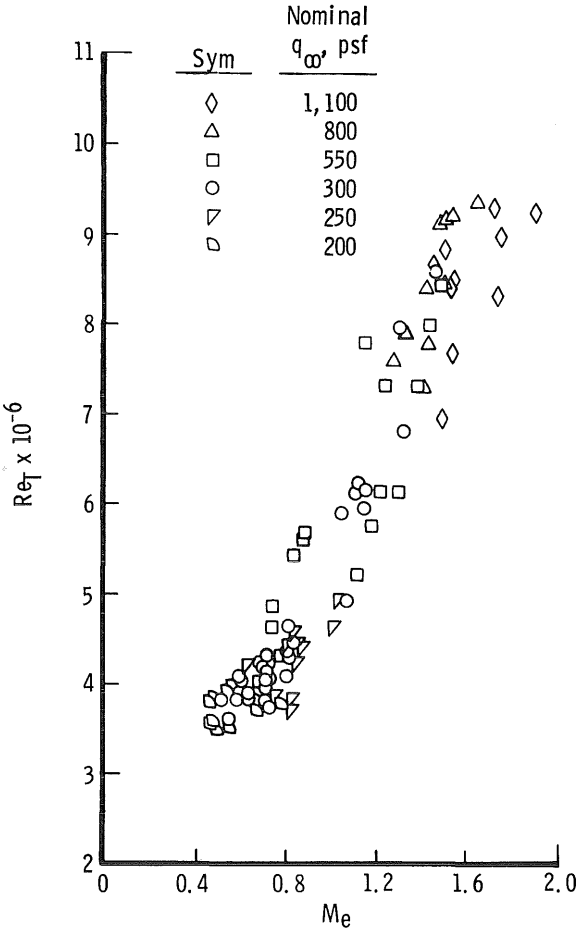

Figure 16. In-flight transition Reynolds number as a function of M_e.

Normalized overall-RMS free-stream impact microphone data acquired in flight are shown in Fig. 17. The data vary monotonically as a function of Mach number and indicate a very low disturbance environment in flight. As shown in Fig. 18, the end-of-transition Reynolds number correlates well with the disturbance measurements under the laminar portion of the boundary layer on the cone surface. (Transition occurred ahead of the forward microphone at the higher values of q_∞, hence no disturbance measurements under a laminar boundary layer could be obtained.) One might expect that these two quantities should be related because the connection between the pressure fluctuations dominated by the growing Tollmien-Schlichting waves and the eventual transition Reynolds number is obvious. However, there also exists a correlation between the transition Reynolds number and the free-stream impact pressure fluctuations as shown in Fig. 19, and it is less obvious why this should be so. No real understanding of precisely what the free-stream impact probe measured was obtained in the flight experiment, nor could the sources of the disturbances actually imposed on the cone be ascertained. The wake of the cone itself represented a significant disturbance source which may have established a disturbance value.

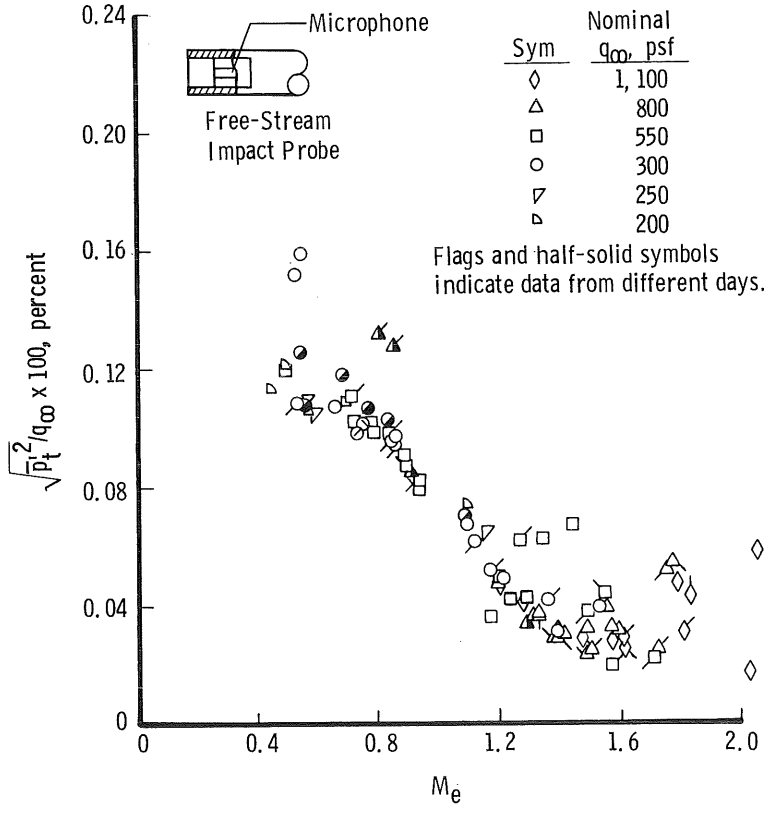

Figure 17. Free-stream impact pressure fluctuations.

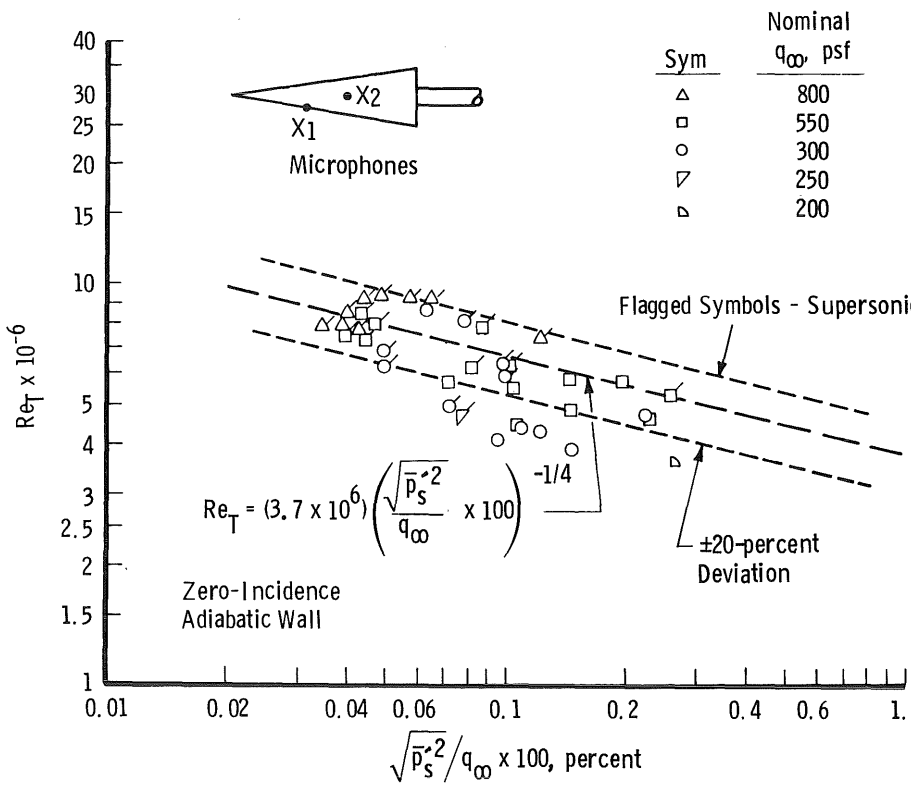

Figure 18. Correlation between flight Re_T and cone surface disturbance measurements.

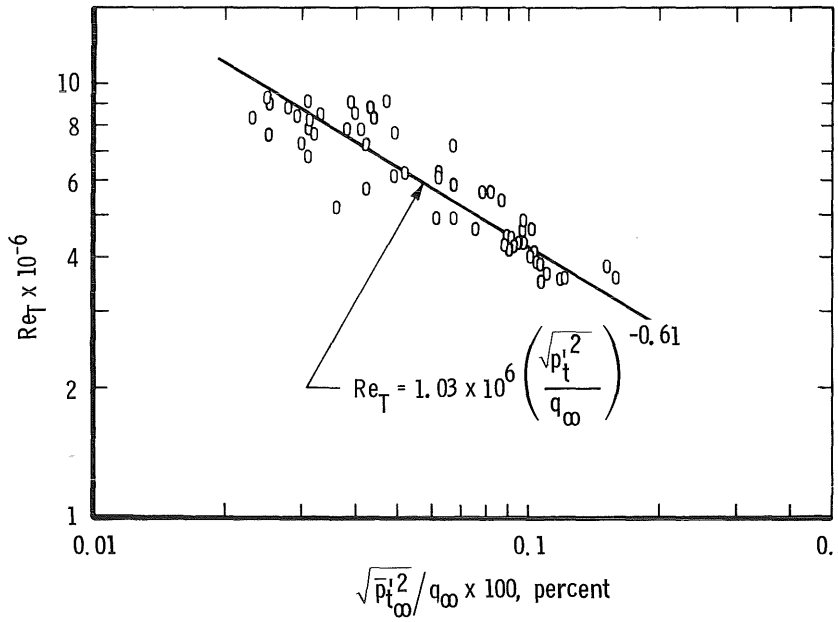

Figure 19. Correlation between flight Re_T and impact probe disturbance measurements.

Only at two Mach numbers were sufficient flight data taken at varied altitudes to check for a unit Reynolds effect in the flight data. The data are presented in Fig. 20. Although the altitude variation in thousands of feet was large, the spread in unit Reynolds number was only about a factor of two. These results are, therefore, not as conclusive as one would like. One might argue that the data indicate a slight increase in Re_T with increase in U_∞/ν_∞ at both Mach numbers. In fact, the slope $\partial R_{e_T}/\partial(U_\infty/\nu_\infty)$ found in the aeroballistic range (Ref. 16) will fit the data presented in Fig. 20 quite well. However, because of the data scatter, no conclusive statement is possible.

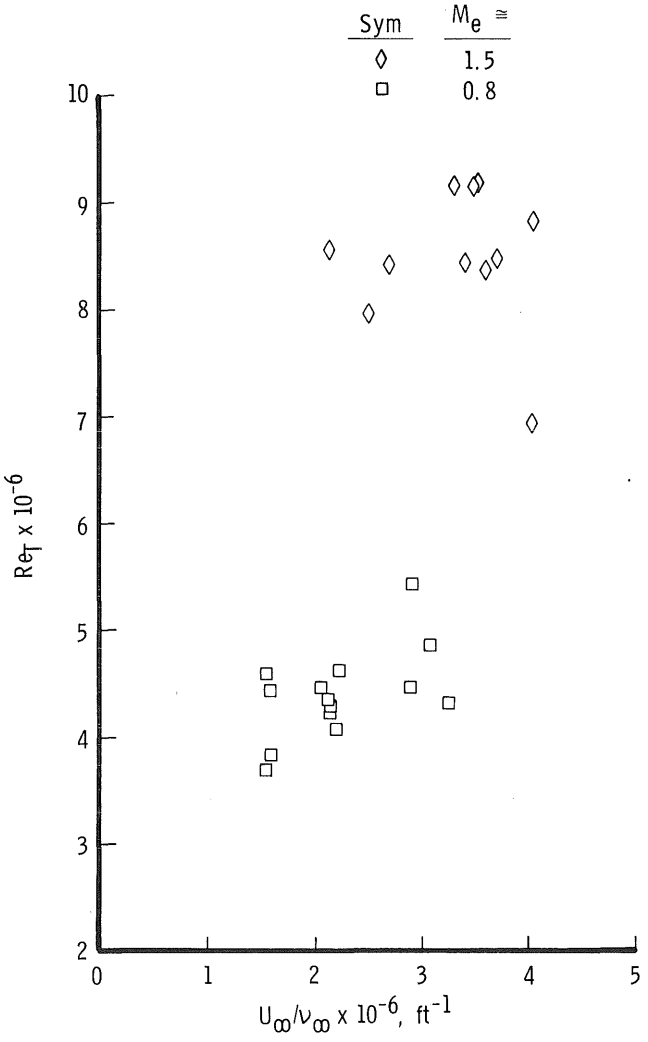

Figure 20. In-flight transition Reynolds number as a function of U_∞/ν_∞.

5.2 WIND TUNNEL DATA

It was possible to distinguish characteristics of transition behavior as a function of M_∞ and U_∞/ν_∞ in four major groupings of tunnels given in Ref. 10. These groupings (see Table 1) were made on the basis of similar wind tunnel geometric configuration. The four groups were as follows:

1. Slotted- or solid-wall transonic and subsonic tunnels,
2. Perforated-wall transonic tunnels,
3. Two-dimensional-nozzle supersonic tunnels, and
4. Sliding-block-nozzle supersonic tunnels

Note that the data presented in Fig. 21 from the Group 2 tunnels with walls taped are mostly below the flight data. As shown in Fig. 21, there is relatively good agreement between the flight and wind tunnel data up to about $M_e = 1.2$ for the Group 1, 3, and 4 tunnels, Fig. 21. Beyond $M_e = 1.5$, however, Re_T in the wind tunnels decreases in constrast to Re_T in flight, which continues to increase. The transition Reynolds numbers measured in all wind tunnel groups, Ref. 10, and the flight data, are compared as a function of M_e in Figs. 21 and 22. The wind tunnel data have been interpolated to nominal unit Reynolds numbers of 2.0×10^6, 3.0×10^6, and 4.0×10^6 ft $^{-1}$. There is a 14-percent increase in Re_T for unit Reynolds numbers between 2 and 4 million at supersonic speeds in the wind tunnels. The flight data envelope is from Fig. 16. There is very poor correlation between Re_T obtained in flight and in the Group 2 tunnels.

The overall RMS pressure fluctuations measured on the cone surface for laminar boundary-layer conditions are shown in Fig. 23 for tunnels which represent some of the lowest values measured in the wind tunnels across the full Mach number range. The dashed curve shown in Fig. 23 is Lowson's empirical relation from Ref. 17,

$$\frac{\sqrt{\overline{p_s'^2}}}{q_\infty} \times 100 = \frac{0.6}{1 + 0.14\, M_\infty^2} \tag{2}$$

for estimating the pressure fluctuations at the wall beneath an attached turbulent boundary layer. The data obtained in wind tunnels represent disturbances perceived at the cone surface from all sources including those generated by the tunnel wall boundary layer. These disturbance values generally lie below Lowson's relation but above the envelope of the flight test data, indicating that in those tunnels the boundary layer is being excited by external

sources whose intensity, while a factor of three above the flight values, is for the most part below that of a fully turbulent boundary layer. Since the transition Reynolds numbers measured in these wind tunnels at Mach numbers below about 1.2 or so agree with flight (within the data scatter), the noise environment must be sufficiently low not to affect transition. Beyond a Mach number of about 1.2, however, even the best wind tunnels are not quiet enough to duplicate the flight data. Thus, data obtained in all tunnels between $M_\infty \approx 1.2$ and some upper boundary, certainly greater than two, are not representative of

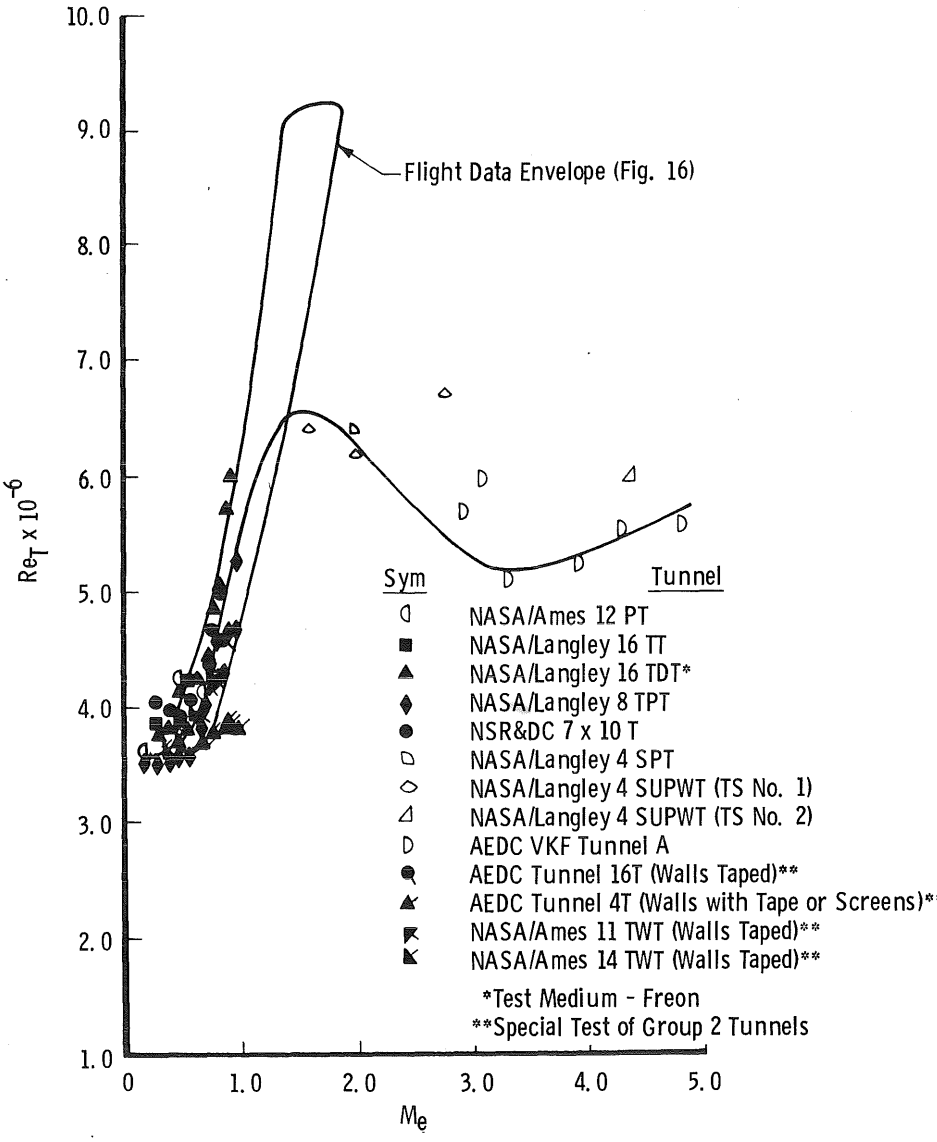

a. $U_\infty/\nu_\infty = 2.0 \times 10^6$

Figure 21. Transition Reynolds numbers obtained in wind tunnel groups 1, 2, and 3.

flight if the phenomenon of interest is dependent on the location of natural boundary-layer transition. In the Group 2 tunnels the disturbance environment is, at some Mach numbers, two orders of magnitude more intensive than the flight values as shown in Fig. 24. The Group 2 tunnels exhibited large increases in $\sqrt{\overline{p}'^2_s}/q_\infty$ in the narrow band of Mach numbers

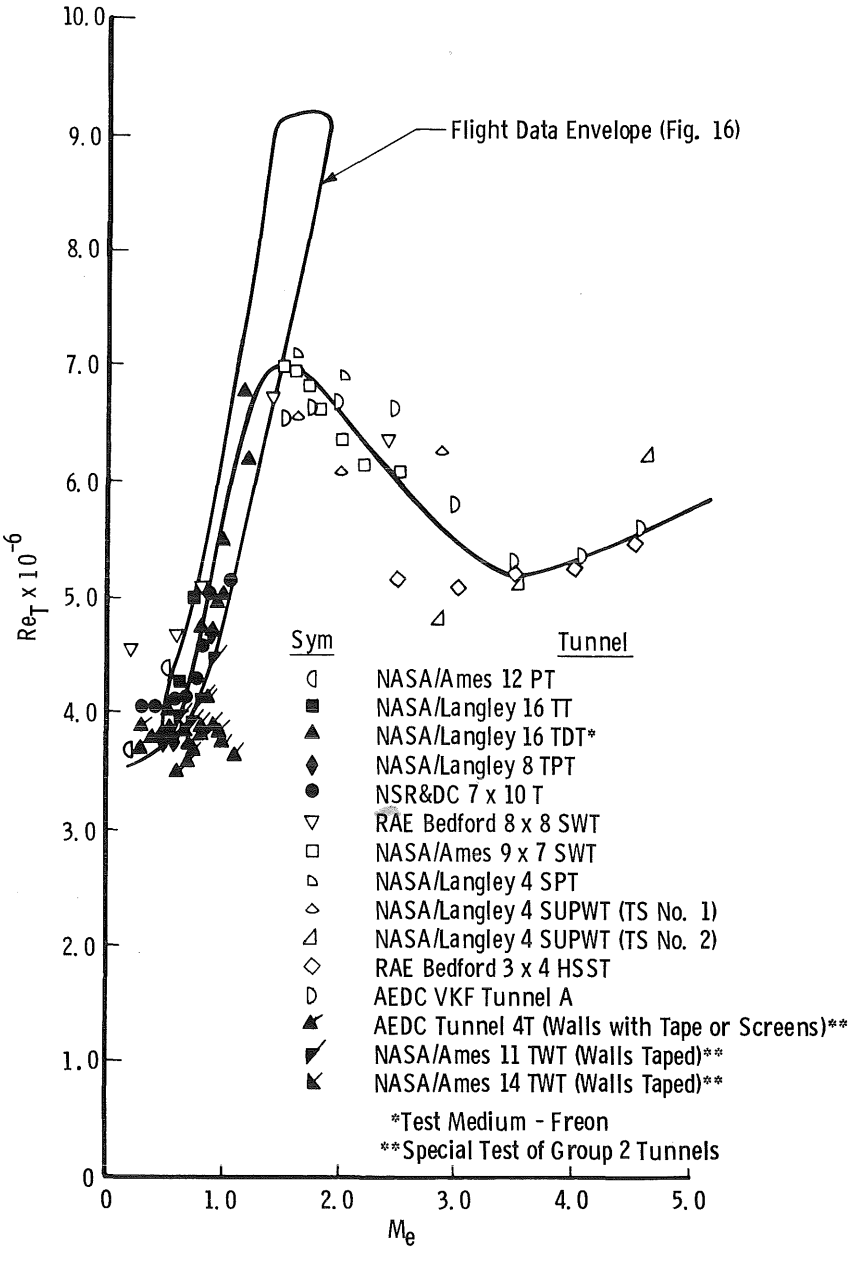

b. $U_\infty/\nu_\infty = 3.0 \times 10^6$

Figure 21. Continued.

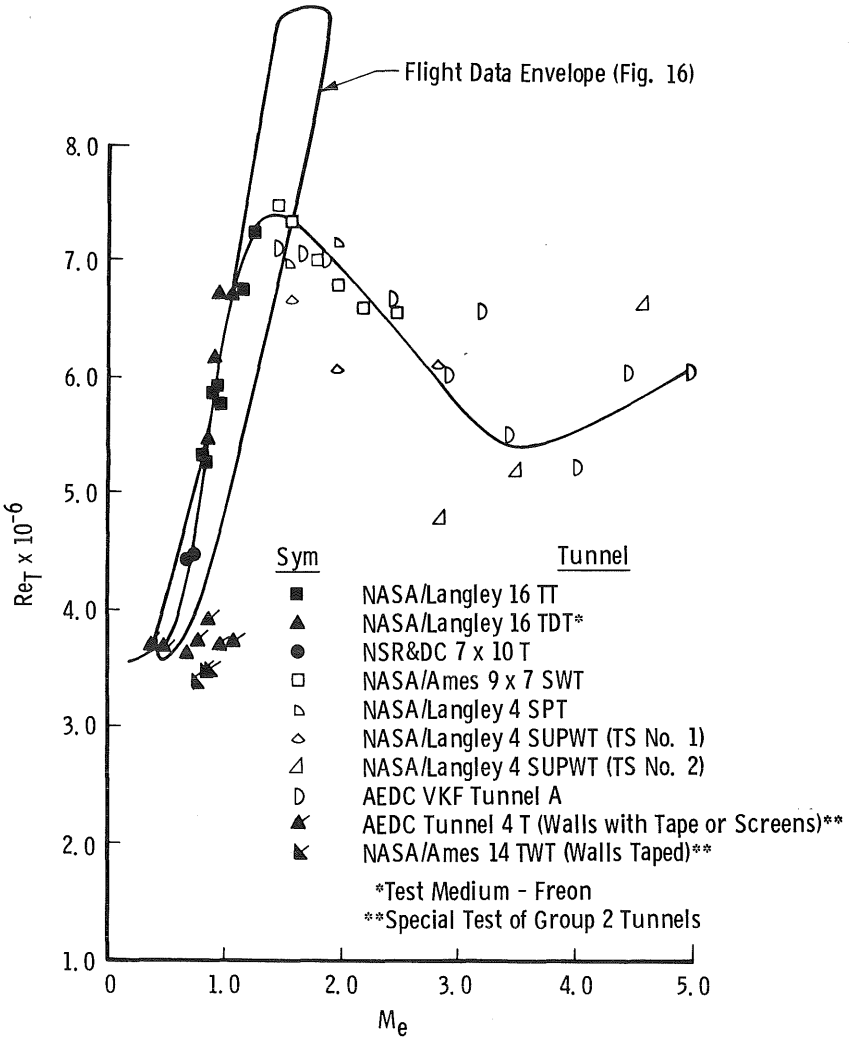

c. $U_\infty/\nu_\infty = 4.0 \times 10^6$

Figure 21. Concluded.

from about 0.6 to 0.9. When $\sqrt{\bar{p}'^2_s}/q_\infty$ was larger than about 1.5 percent, transition was so far forward on the cone that both microphones were beneath either turbulent or transitional flow.

A correlation of Re_T meaurements as a function of measured $\sqrt{\bar{p}'^2_s}/q_\infty$ in eighteen of the wind tunnels and in flight is presented in Fig. 25. (These are the same flight data shown in Fig. 18.) This correlation includes data at all Mach numbers and unit Reynolds numbers. The data appear to fall within approximately ±20 percent of a mean empirical curve given by

$$Re_T = 3.7 \times 10^6 \left[\sqrt{\bar{p}'^2_s}/q_\infty \times 100 \right]^{-1/4} \quad (3)$$

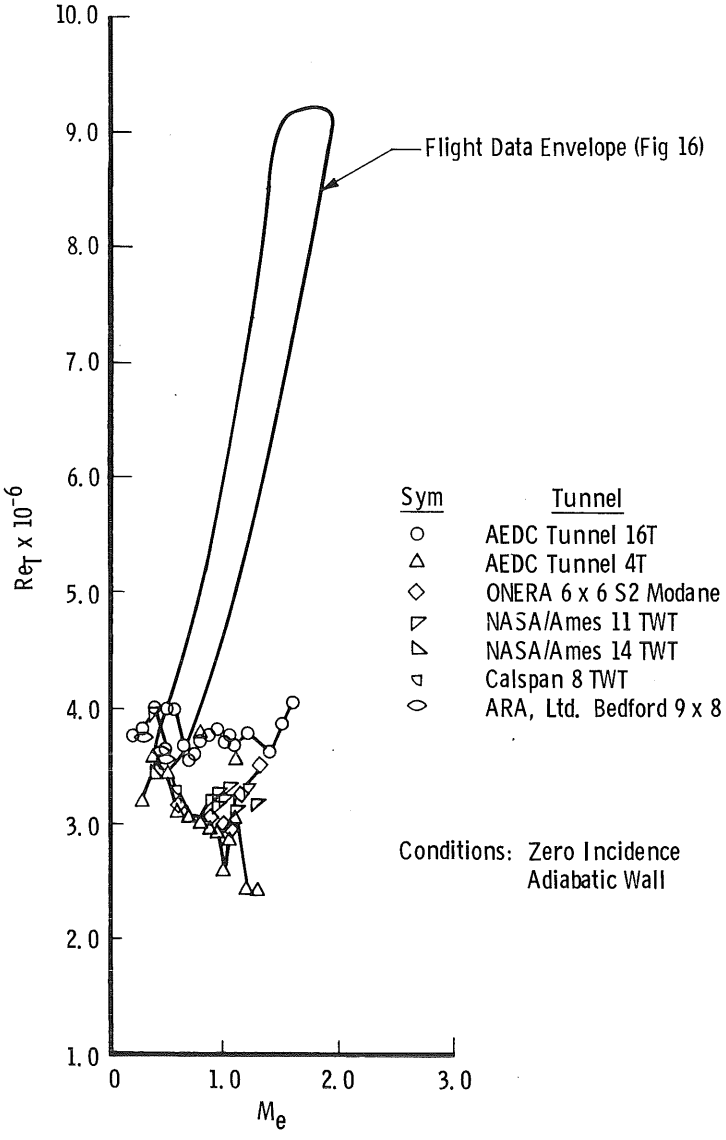

a. $U_\infty/\nu_\infty = 2.0 \times 10^6$

Figure 22. Transition Reynolds numbers in group 2 wind tunnels.

The term $\sqrt{\overline{p_s'^2}}$ was measured under the laminar portion of the cone boundary and, of course, includes an integration of all frequencies above 200 Hz from all sources including the cone boundary layer itself. The need to obtain spectral data in the 10- to 80-kHz range was not recognized during the wind tunnel investigations (nor is it an easy measurement to obtain). Thus, one can only speculate that "early" transition is caused by external excitation

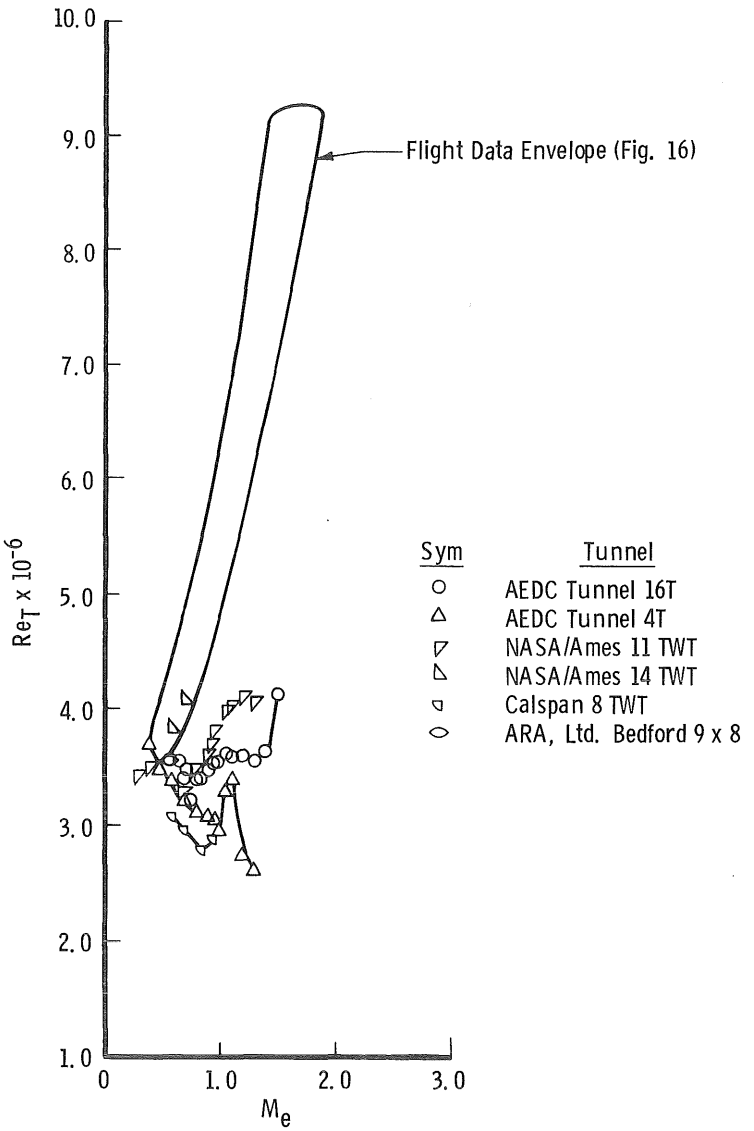

b. $U_\infty/\nu_\infty = 3.0 \times 10^6$

Figure 22. Continued.

of the boundary layer at frequencies associated with the "Tollmien-Schlichting" waves, wherein the more energy contained in the unstable frequency band the earlier transition occurs. The data presented in Fig. 25, however, do not refute that hypothesis. It is also possible, however, that large values of sound power at frequencies lower than those associated with the "natural" waves may cause transition through another mechanism — for example, some sort of nonlinear coupling phenomenon (i.e., see Ref. 18 by M. Morkovin).

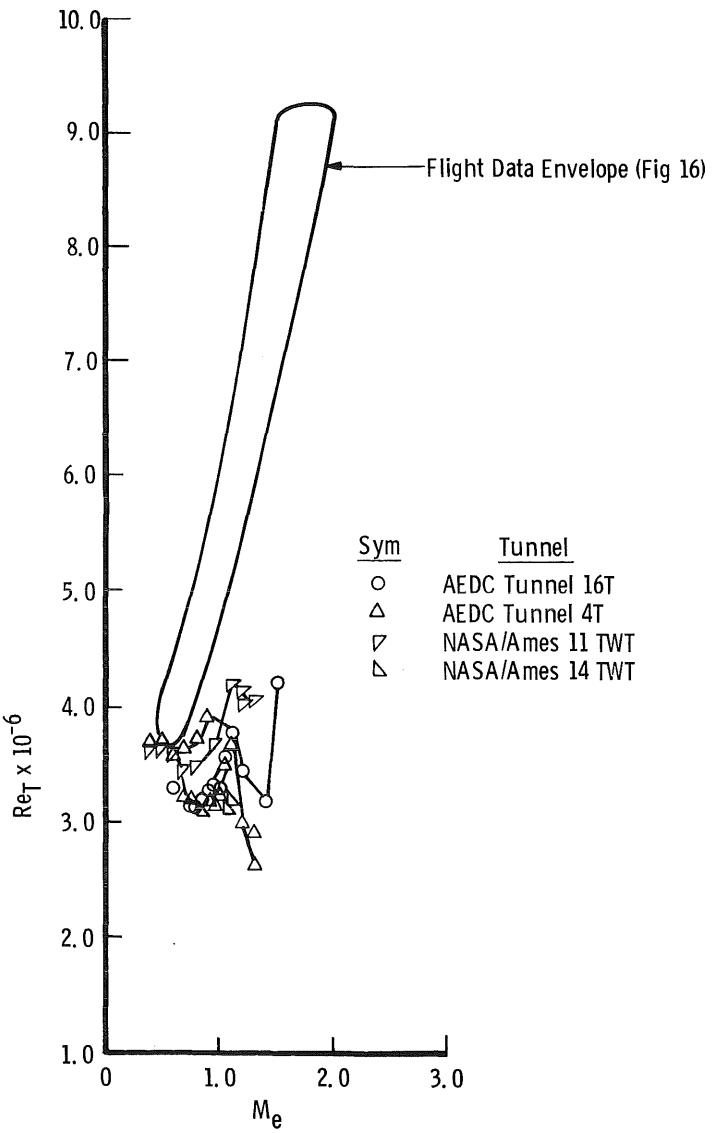

c. $U_\infty/\nu_\infty = 4.0 \times 10^6$

Figure 22. Concluded.

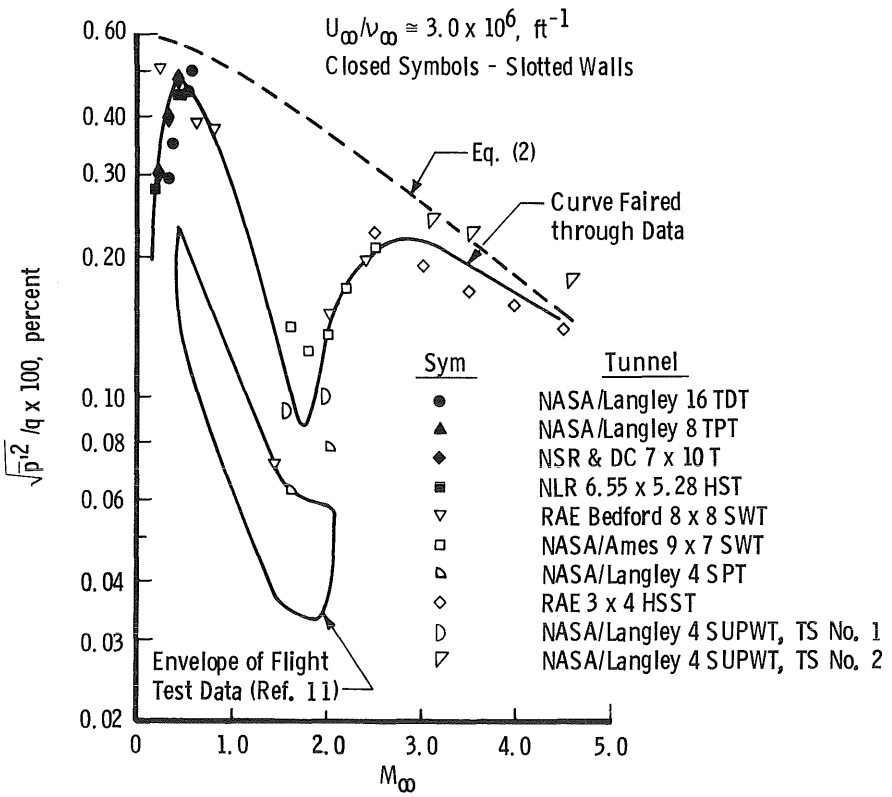

Figure 23. Comparison of lowest disturbance levels measured in wind tunnels with disturbances in flight.

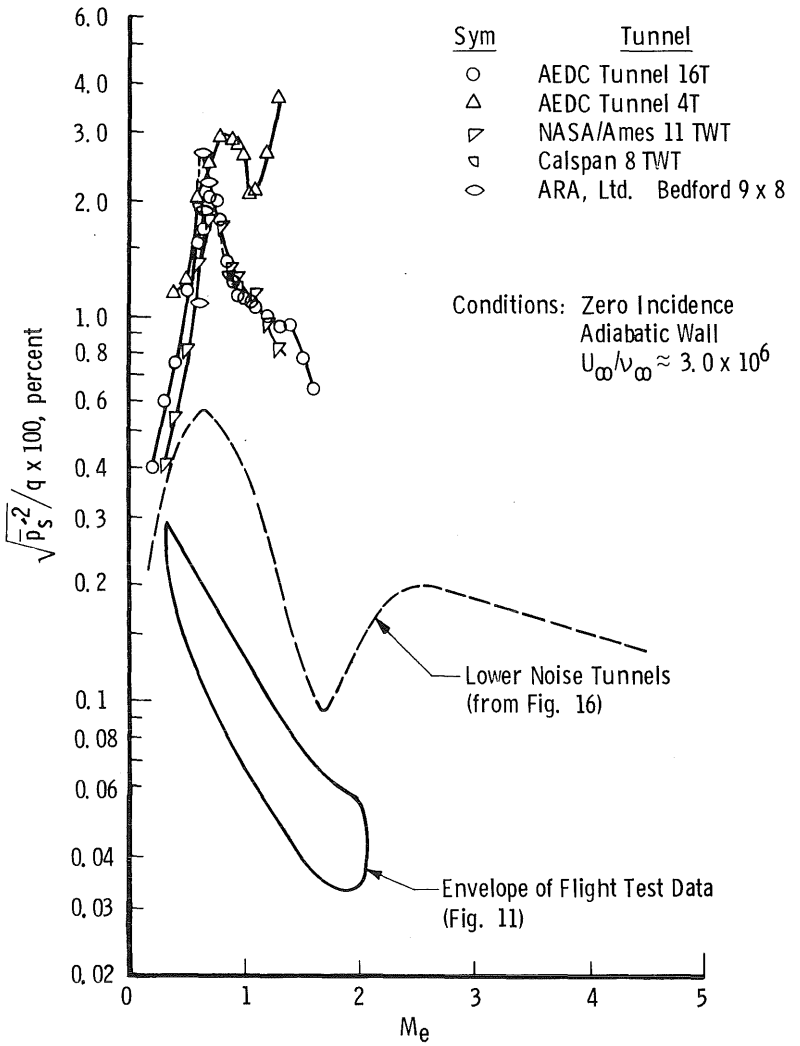

Figure 24. Disturbance measurements in group 2 transonic wind tunnels.

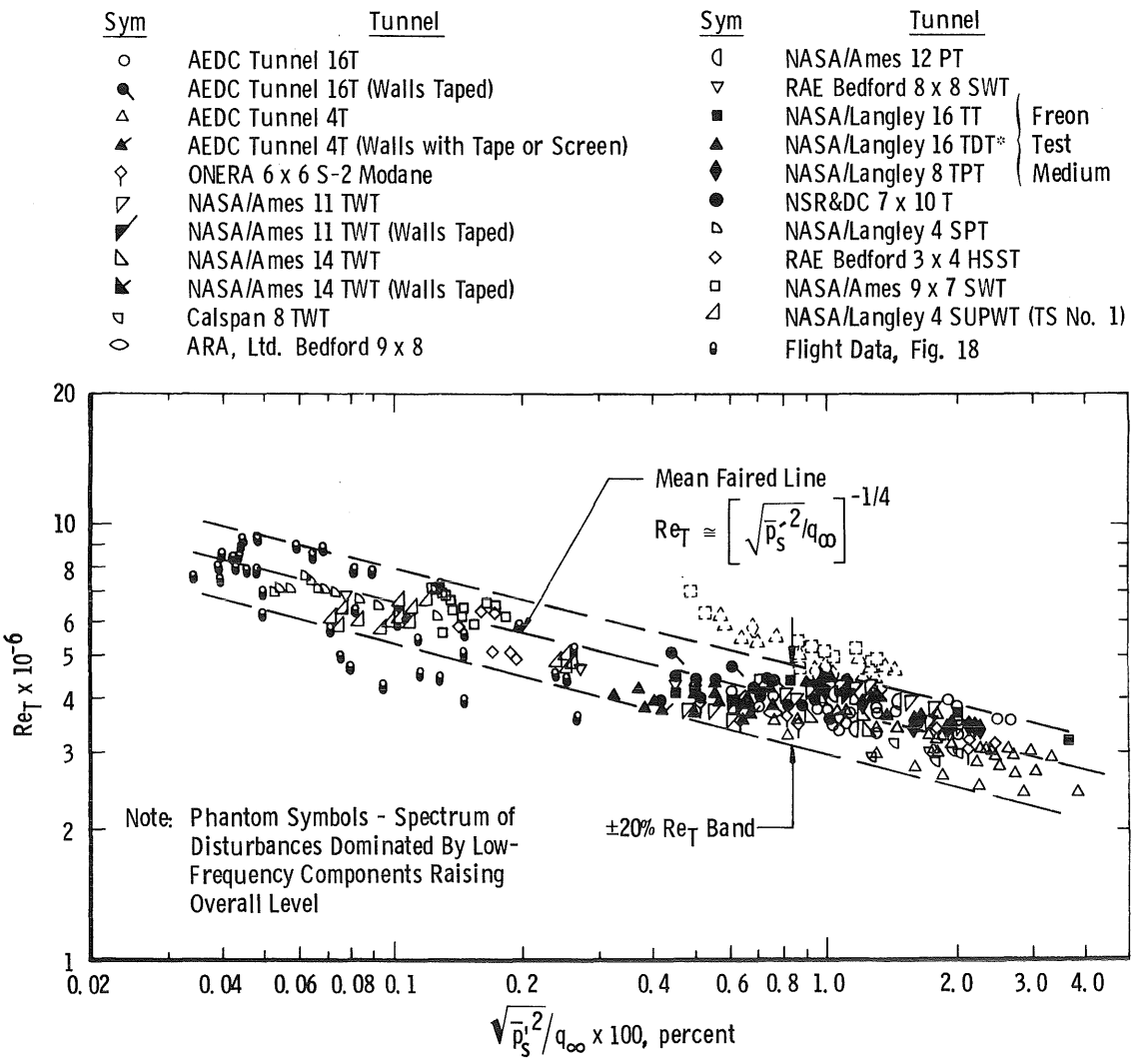

Figure 25. Correlation between Re_T and cone surface disturbance measurements.

6.0 CONCLUDING REMARKS

An experimental investigation using a 10-deg (total angle) calibration cone with standardized instrumentation and test procedures was conducted to gain increased understanding of the nature of free-stream disturbances in wind tunnels and what influence they have on Reynolds number scaling. The investigation included tests in 23 wind tunnels in the U. S. and Europe and flight tests with the cone mounted on the nose of an F-15 aircraft.

The approach was to use the laminar/turbulent transition location on the cone to determine the influence of the noise and turbulence in the free stream on transition location and to determine whether a correlation existed between transition Reynolds number and the noise environment.

The data indicated that the mechanism causing transition in both flight and the wind tunnels is associated with the formation of Tollmien-Schlichting waves in the laminar boundary layer. The end-of-transition Reynolds number in both flight and the wind tunnels was found to be primarily a function of the noise measured at the cone surface in terms of the RMS fluctuating pressure measured under the laminar portion of the boundary layer and normalized by the free-stream dynamic pressure. Within ± 20 percent the variation of transition Reynolds number with the noise parameter was independent of Mach number and unit Reynolds number. Thus, it follows that the variation of Re_T with Mach number and unit Reynolds number is directly related to the variation of the noise as a function of Mach number and unit Reynolds number, at least over the range of this investigation. In those tunnels which operate at Mach numbers below about 1.2 and whose free-stream-borne acoustical disturbances are lower in amplitude than the disturbances produced by a turbulent boundary layer, transition Reynolds numbers agreed with those obtained in flight. At Mach numbers above about 1.4, none of the tunnels produced transition Reynolds numbers which agreed with flight.

REFERENCES

1. Potter, J. L. and Whitfield, J. D. "Preliminary Study of the Effect of Unit Reynolds Number on Transition Sensitive Data." AEDC-TN-57-37 (AD135338), September 1957.

2. Morkovin, M. V. "Instability, Transition to Turbulence, and Predictability." Opening Address, AGARP-CP-224, AGARD Fluid Dynamics Panel Symposium on Laminar-Turbulent Transition, Lyngby, Denmark, May 2-4, 1977.

3. Treon, S. L., Steinle, F. W., Jr., Hagerman, J. R., et al. "Further Correlation of Data from Investigations of a High-Subsonic-Speed Transport Aircraft Model in Three Major Transonic Wind Tunnels." AIAA Paper No. 71-291, AIAA 6th Aerodynamic Testing Conference, Albuquerque, New Mexico, March 10-12, 1971.

4. Credle, O. P. and Carleton, W. E. "Determination of Transition Reynolds Number in the Transonic Mach Number Range." AEDC-TR-70-218 (AD875995), October 1970.

5. Dougherty, N. S., Jr. and Steinle, F. W., Jr. "Transition Reynolds Number Comparisons in Several Major Transonic Tunnels." AIAA Paper No. 74-627, AIAA 8th Aerodynamic Testing Conference, Bethesda, Maryland, July 8-10, 1974.

6. Vaucheret, X. "Acoustic Fluctuations Generated by the Ventilated Walls of a Transonic Wind Tunnel." Paper No. 25, AGARD Fluid Dynamics Panel Symposium on Wind Tunnel Design and Testing Techniques, London, England, October 6-8, 1975, AGARD CP No. 174; also ONERA Chatillon TP No. 1324, 1974.

7. Ross, R. and Rohne, P. B. "The Character of Flow Unsteadiness and Its Influence on Steady-State Transonic Wind Tunnel Measurements." Paper No. 45 in AGARD-CP-174, AGARD Fluid Dynamics Panel Symposium on Wind Tunnel Design and Testing Techniques, London, England, October 6-8, 1975; also NLR Amsterdam TR 74128 U, August 1973.

8. Mabey, D. B. "Boundary-Layer Transition Measurements on the AEDC 10° Cone in Three RAE Wind Tunnels and Their Implications." British ARC R&M 3821, RAE-TR-76077, June 1976.

9. Jordan, R. "Tests with the AEDC 10-Deg Transition Cone in the 9×8 Ft Transonic Tunnel." ARA, Ltd. Model Test Note Z.32, April 1973.

10. Dougherty, N. S., Jr. "Influence of Wind Tunnel Noise on the Location of Boundary-Layer Transition on a Slender Cone at Mach Numbers from 0.2 to 5.5." AEDC-TR-78-44, 1980.

11. Fisher, D. F. and Dougherty, N. S., Jr. "In-Flight Measurements of Boundary-Layer Transition on a 10-Deg Cone at Mach numbers from 0.5 to 2.0." NASA TP, 1980.

12. Mack, L. M. "Boundary-Layer Stability Theory." JPL/CIT TR 900-277, June 1969.

13. Potter, J. Leith and Whitfield, J. D. "Effects of Slight Nose Bluntness and Roughness on Boundary-Layer Transition in Supersonic Flows." *Journal of Fluid Mechanics*, Vol. 12, Part 4, April 1962, pp. 501-535.

14. Pate, S. R. and Schueler, C. J. "Effects of Radiated Aerodynamic Noise on Model Boundary-Layer Transition in Supersonic and Hypersonic Wind Tunnels." AEDC-TR-67-236 (AD666644), March 1969; also *AIAA Journal*, Vol. 7, March 1969, pp. 450-457.

15. Pate, S. R. "Measurements and Correlations of Transition Reynolds Numbers on Sharp Slender Cones at High Speeds." AEDC-TR-69-172 (AD698326), December 1969; also AIAA Paper No. 70-799, AIAA 3rd Fluid and Plasma Dynamics Conference, Los Angeles, California, June 29–July 1, 1970.

16. Potter, J. L. "Boundary-Layer Transition on Supersonic Cones in an Aeroballistic Range." AIAA *Journal*, Vol. 13, No. 3, March 1975, pp. 270-277.

17. Lowson, M. V. "Prediction of Boundary-Layer Presssure Fluctuations." AFFDL-TR-67-167, April 1968.

18. Morkovin, M. "Critical Evaluation of Transition from Laminar to Turbulent Shear Layers with Emphasis on Hypersonically Traveling Bodies." AFFDL-TR-68-149, March 1969.

NOMENCLATURE

F	Nondimensional frequency, Eq. (1)
f	Frequency, Hz
G(f)	Power spectral function over 30-sec averaging time, $\overline{psf}^2$/Hz
L	Cone surface length, 44.5 in.
p	Pressure, psf
$\bar{p}'$	Averaged pressure fluctuation, psf
$\sqrt{\bar{p}'^2}$	Root-mean-square pressure fluctuation, $\left[\int_0^f G(f)df\right]^{1/2}$
q	Dynamic pressure, psf
Re_T	End-of-transition Reynolds number
Re_t	Onset-of-transition Reynolds number at $x = X_t$
Re_x	Reynolds number along cone ray for x measured from cone apex
T	Temperature, °R
t	Time, sec
U	Velocity, ft/sec
U/ν	Reynolds number per unit length, ft^{-1}
X_T	End-of-transition location in cone boundary layer, ft
X_t	Onset-of-transition location in cone boundary layer, ft
x	Surface length on cone ray from apex, ft
α	Angle of attack, deg

β Angle of yaw, deg

θ_c Cone half angle, 5 deg

ν Kinematic viscosity, ft^2/sec

ϕ Cone roll angle from windward stagnation ray to the pitot probe, $\tan^{-1}(\beta/\alpha)$ -180, deg

ψ Angle in which disturbance propagates in a laminar boundary layer relative to the stream direction, deg

SUBSCRIPTS

0 Zero incidence condition

1 Cone forward microphone location, 18.0 in. from the apex

2 Cone aft microphone location, 26.0 in. from the apex

aw Adiabatic wall

e Boundary-layer edge conditions

s Cone surface conditions

t Total conditions

w Wall conditions

∞ Free-stream conditions